The Astrophysical Journal, 568:878–900, 2002 April 1

RXTE OBSERVATIONS OF THE NEUTRON STAR LOW-MASS X-RAY BINARY GX 17+2: CORRELATED X-RAY SPECTRAL AND TIMING BEHAVIOR

Jeroen Homan,[1,2] Michiel van der Klis,[1] Peter G. Jonker,[1] Rudy Wijnands,[3,4]
Erik Kuulkers,[5,6] Mariano Méndez,[7] and Walter H. G. Lewin[8]
Received 2001 April 19; accepted 2001 December 7

ABSTRACT

We have analyzed ~600 ks of *Rossi X-Ray Timing Explorer* data of the neutron star low-mass X-ray binary and Z source GX 17+2. A study was performed of the properties of the noise components and quasi-periodic oscillations (QPOs) as a function of the broadband spectral properties, with the main goal to study the relation between the frequencies of the horizontal branch (HBO) and upper kHz QPOs. It was found that when the upper kHz QPO frequency is below 1030 Hz these frequencies correlate, whereas above 1030 Hz they anticorrelate. GX 17+2 is the first source in which this is observed. We also found that the frequency difference of the high-frequency QPOs was not constant and that the quality factors (Q-values) of the HBO, its second harmonic, and the kHz QPOs are similar and vary almost hand in hand by a factor of more than 3. Observations of the normal branch oscillations during two type I X-ray bursts showed that their absolute amplitude decreased as the flux from the neutron star became stronger. We discuss these and other findings in terms of models that have been proposed for these phenomena. We also compare the behavior of GX 17+2 and other Z sources with that of black hole sources and consider the possibility that the mass accretion rate might not be the driving force behind all spectral and variability changes.

Subject headings: accretion, accretion disks — stars: individual (GX 17+2) — X-rays: individual (GX 17+2) — X-rays: stars

1. INTRODUCTION

Based on their broadband spectral and variability properties, six of the persistently bright neutron star low-mass X-ray binaries (LMXBs) were classified as Z sources (Hasinger & van der Klis 1989), after the Z-like tracks they trace out in X-ray color-color diagrams (CDs) and hardness-intensity diagrams (HIDs). These sources are GX 17+2, Cyg X-2, GX 5−1, GX 340+0, Sco X-1, and GX 349+2. The Z-like tracks roughly consist of three branches, which, from top to bottom, are referred to as the horizontal branch (HB), the normal branch (NB), and the flaring branch (FB). It is generally believed that the parameter that determines the position along the Z track is the mass accretion rate, increasing from the HB to the FB. Note that the definition of the mass accretion rate in this respect is rather vague—it is often defined as the mass accretion rate through the inner disk and onto the neutron star surface. In addition to spectral changes along the Z track, some of the Z sources show long-term changes in the shape and position of the Z track in the CD and HID. These secular changes, as they are referred to, are clearly observed in Cyg X-2 (Kuulkers, van der Klis, & Vaughan 1996; Wijnands et al. 1997b), GX 5−1 (Kuulkers et al. 1994), and GX 340+0 (Kuulkers & van der Klis 1996) (the Cyg-like sources; the other Z sources are referred to as the Sco-like sources) and more recently also in GX 17+2 (Wijnands et al. 1997a). It has been suggested that they are related to the relatively high inclination at which these sources are seen (Kuulkers et al. 1994; Kuulkers & van der Klis 1995) or to different magnetic field strengths of the neutron stars (Psaltis, Lamb, & Miller 1995).

The power spectra of the Z sources show several types of quasi-periodic oscillations (QPOs) and noise components (see van der Klis 1995a for a review). It was found that their presence and properties are very well correlated with the position of the source along the Z track (Hasinger & van der Klis 1989), even when the Z tracks show secular changes (e.g., Kuulkers et al. 1994). Three types of low-frequency (<100 Hz) QPOs are seen in the Z sources: the horizontal branch (HBOs), normal branch (NBOs) and flaring branch QPOs (FBOs). Their names derive from the branches on which they were originally found. The HBO is found on the HB and NB with a frequency (15–60 Hz) that gradually increases along the HB toward the NB. When the sources move from the HB onto the NB, the frequency increase flattens off. In GX 17+2 and Cyg X-2, it was found that when the source passes a certain point on the NB, the HBO frequency starts to decrease (Wijnands et al. 1996, 1997b). The NBO and FBO are most likely the same phenomenon. They are found on the NB and FB (near the NB/FB vertex) but not on the HB. On the NB the QPO has a frequency of ~5–7 Hz, which rapidly increases to ~20 Hz when the source

[1] Astronomical Institute "Anton Pannekoek," University of Amsterdam, and Center for High Energy Astrophysics, Kruislaan 403, 1098 SJ Amsterdam, Netherlands; homan@astro.uva.nl, michiel@astro.uva.nl, peterj@astro.uva.nl.
[2] Current address: Osservatorio Astronomico di Brera, Via E. Bianchi 46, 23807 Merate LC, Italy; homan@merate.mi.astro.it.
[3] Center for Space Research, Massachusetts Institute of Technology, 77 Massachusetts Avenue, Cambridge, MA 02139-4307; rudy@space.mit.edu.
[4] Chandra Fellow.
[5] Space Research Organization Netherlands, Sorbonnelaan 2, 3584 CA Utrecht, Netherlands; e.kuulkers@sron.nl.
[6] Astronomical Institute, Utrecht University, P.O. Box 80000, 3508 TA Utrecht, Netherlands.
[7] Facultad de Ciencias Astronómicas y Geofísicas, Universidad Nacional de La Plata, Paseo del Bosquey S/N, 1900 La Plata, Argentina; m.mendez@sron.nl.
[8] Department of Physics and Center for Space Research, Massachusetts Institute of Technology, 77 Massachusetts Avenue, Cambridge, MA 02139-4307; lewin@space.mit.edu.

moves across the NB/FB vertex (Priedhorsky et al. 1986; Dieters & van der Klis 2000). In recent years two high-frequency (or kHz) QPOs were found in the Z sources (van der Klis et al. 1996; Wijnands et al. 1997a, 1998a, 1998b; Jonker et al. 1998; Zhang, Strohmayer, & Swank 1998; see van der Klis 2000 for a review). They are often observed simultaneously, with a frequency difference of ~300 Hz, and have frequencies between 215 and 1130 Hz, which increase from the HB to the NB. In Sco X-1 the frequency difference was found to decrease with increasing QPO frequency (van der Klis et al. 1997b). The frequency difference in the other Z sources is consistent both with the behavior seen in Sco X-1 and with being constant (Wijnands et al. 1997a; Jonker et al. 1998; Psaltis et al. 1998). Three types of noise are seen in the Z sources. They are the very low frequency noise (VLFN), the low-frequency noise (LFN), and the high-frequency noise (HFN). The VLFN and HFN are found on all branches, whereas the LFN is observed only on the HB and NB. The VLFN, which is found at frequencies below 1 Hz, can be described by a power law. The HFN and LFN are both band-limited components, with cutoff frequencies of, respectively, 10–100 Hz and 2–10 Hz.

Many competing models have been proposed for the origin of the QPOs and noise components. It is beyond the scope of this introduction to mention these models in detail—most of them will be discussed in § 4.

In this paper we present a study, based on data acquired with the *Rossi X-Ray Timing Explorer* (*RXTE*), of the correlated spectral and variability properties of the Z source GX 17+2. It is a continuation of the work by Wijnands et al. (1996, 1997a). The current paper constitutes the first report on the very large observing campaign of 1999, which more than doubled the total coverage of the source. This campaign was undertaken with the express purpose of investigating if a nonmonotonic relation exists between the frequency of the kHz QPOs and the HBO in GX 17+2. Section 2 deals with the observations and analysis. The spectral results are presented in § 3.1 and the results for each power spectral component in §§ 3.2 and 3.3. A number of qualitatively new results are found in our greatly expanded data set. In particular, we find that when the upper kHz QPO frequency is below 1030 Hz, it correlates with the HBO frequency, whereas above 1030 Hz they anticorrelate. We also find that the kHz QPO frequency difference is not constant and that the Q-values of the HBO and kHz QPOs are probably not explained by lifetime broadening. These and other results are compared to observations of other Z sources and discussed in terms of current models in § 4. Finally, we argue that changes in the spectral and variability properties of the Z sources may not be not driven by changes in the mass accretion rate.

2. OBSERVATIONS AND ANALYSIS

The data used for the analysis in this paper were all obtained with the Proportional Counter Array (PCA; Jahoda et al. 1996) on board *RXTE* (Bradt, Rothschild, & Swank 1993). The PCA consists of five xenon-filled proportional counter units (PCUs), each with an effective area of ~1250 cm^2 (at 10 keV). Although the five PCUs are in principle identical, they each have a slightly different energy response. These responses change continuously because of slow processes such as gas leakage and the aging of the electrodes. In addition, the high voltage settings of the instruments are occasionally altered (gain changes), resulting in rather more drastic changes in the detector response. These changes have, at the time of writing, been applied three times during the lifetime of *RXTE*, thereby defining four gain epochs. Occasionally, one or more PCUs are not operational. They can be switched off by an internal safety mechanism or by the ground control crew, for reasons of detector preservation. Therefore, the number of active detectors varies between the observations.

All our *RXTE*/PCA observations of GX 17+2 were done between 1997 February 2 and 2000 March 31. A log of the observations is given in Table 1. We do not include the observations done in February 1996, which were used by Wijnands et al. (1996). The reasons for this are the limited time resolution in the energy range of interest and difficulties with scaling the S_z (see below) due to an incomplete Z track. Data taken during satellite slews and Earth occultations were removed. The nine type I X-ray bursts that were observed are the subject of a separate article by Kuulkers et al. (2001); two of those were also studied in this paper. The total amount of good data that remained was ~600 ks.

Data were collected in several modes with different time and spectral resolutions. Two of these modes, "Standard 1" and "Standard 2," were always operational. In addition to these two modes, other modes were active that varied

TABLE 1
A Log of All *RXTE*/PCA Observations Used in This Paper

Begin Time (UTC)	End Time (UTC)	Total (ks)	Modes[a]	Gain Epoch
1997 Feb 2 19:13.....	1997 Feb 27 03:34	58.7	3 or 4, 5, 6, 9	3
1997 Apr 1 19:13	1997 Apr 4 23:26	34.6	4, 5, 6, 9	3
1997 Jul 27 02:13	1997 Jul 28 00:33	42.9	4, 5, 6, 9	3
1998 Aug 7 06:40.....	1998 Aug 8 23:40	71.0	4, 5, 8	3
1998 Nov 18 06:42.....	1998 Nov 20 13:31	86.0	4, 5, (7), 8	3
1999 Oct 3 02:43.....	1999 Oct 12 07:05	297.6	10, 11, 12	4
2000 Mar 31 12:15.....	2000 Mar 31 16:31	6.9	10, 11, 12	4

Notes.—Mode 7 was not always active during the 1998 November observations. Note that none of the observations represents an uninterrupted interval. Each is a collection of observations that were done around the same time. These observations were separated in time from each other for various reasons, such as Earth occultations, passages of the South Atlantic Anomaly, or observations of other sources.

[a] Modes in addition to the Standard 1 and Standard 2 modes. See Table 2 for modes.

TABLE 2
NAMES AND SETTINGS OF THE DATA MODES THAT WERE USED IN OUR ANALYSIS

Mode	Name	Time Resolution (s)	Energy Range (keV)	Energy Channels
1.....	Standard 1	2^{-3}	2–60	1
2.....	Standard 2	2^{4}	2–60	129
3.....	E_8us_8A_0_1s	2^{-17}	2–60	8
4.....	SB_125us_0_13_1s	2^{-13}	2–5.1	1
5.....	SB_125us_14_17_1s	2^{-13}	5.1–6.6	1
6.....	SB_125us_18_23_1s	2^{-13}	6.6–8.7	1
7.....	SB_125us_18_249_1s	2^{-13}	6.6–60	1
8.....	E_16us_64M_18_1s	2^{-16}	6.6–60	64
9.....	SB_125us_24_249_1s	2^{-13}	8.7–60	1
10.....	SB_125us_0_13_1s	2^{-13}	2–5.8	1
11.....	SB_125us_14_17_1s	2^{-13}	5.8–7.5	1
12.....	E_16us_64M_18_1s	2^{-16}	7.5–60	64

NOTES.—The lower and upper energy boundaries of the PCA energy sensitivity range are given as 2 and 60 keV, although they changed between (and also slightly during) the different gain epochs.

between the observations. The properties of all modes are given in Table 2.

The Standard 2 data were used to perform a broadband spectral analysis. The data were background subtracted, but no dead-time corrections were applied; these were on the order of 2%–5%.

For each 16 s data segment (i.e., the intrinsic resolution of the Standard 2 mode) we defined two colors, which are the ratios of count rates in two different energy bands, and an intensity, which is simply the count rate in one energy band. The energy bands used for the colors (soft and hard color) and intensity are given in Table 3. The lower energy boundaries for the soft color and intensity were chosen relatively high in order to avoid the lowest and least reliable energy channels. By plotting the two colors against each other, a color-color diagram was produced. A hardness-intensity diagram was produced by plotting the hard color against the intensity. To produce the CDs and HIDs, we used only data obtained with those PCUs that (for each gain epoch) were always on. For gain epoch 3, these were PCUs 0, 1, and 2, and for gain epoch 4, PCUs 0 and 2. Because of the different numbers of detectors and the differences in the detector settings, we decided to produce the CDs and HIDs separately for the two gain epochs. However, in choosing the energy channels we tried to take channels whose energy boundaries were as close as possible.

Because of the aging processes mentioned earlier, observations with the same source spectrum that are made more than a few weeks apart end up at different locations in the CD. To correct for this effect, we analyzed a number of *RXTE*/PCA observations of the Crab pulsar/nebula (which is assumed to have a constant spectrum; see also Kuulkers et al. 1994) that were taken around the time of our GX 17+2 observations. For all Crab observations, we produced the colors in the same energy bands that we used for GX 17+2. We found that the observed colors of the Crab indeed changed. For each observation we calculated multiplicative scaling factors, for both colors, with respect to those of the first Crab observation. We used these factors to scale the colors of the GX 17+2 observations back to those of the first GX 17+2 observation. This procedure could be applied only to the epoch 3 observations, where, as expected, we found it to result in a narrower track in the CD. No corrections were applied for the intensity. Since no Crab observations were available for the 2000 March observations, no corrections could be applied to epoch 4 data. The shifts in that data set appeared to be small anyway.

Our power spectral analysis was based on selecting observations as a function of the position along the Z track in the CD. We used a method that is based on the "rank number" and "S_z" parameterization methods introduced by Hasinger et al. (1990) and Hertz et al. (1992), which have been gradually refined in similar studies (Kuulkers et al. 1994, 1997; Kuulkers & van der Klis 1996; Wijnands et al. 1997b; Dieters & van der Klis 2000). In this method in its current form, all points in the CD are projected onto a bicubic spline (see Press et al. 1992) whose normal points are placed by hand in the middle of the Z track (see Fig. 1). The HB/NB and NB/FB vertices are given the values $S_z = 1$ and $S_z = 2$, respectively. The rest of the Z track is scaled according to the length of the NB. Problems arise when sharp curves are present in the track, in our study most notably around the NB/FB vertex. Because of scatter, points which have FB properties end up on the NB and vice versa. This is not a problem that is intrinsic only to the S_z parameterization; it is a limitation that applies to all selection methods based on colors. No observable parameter, apart from the power spectra, has been identified that could be used to distinguish NB and FB observations around the vertex better than the X-ray colors.

In order to improve on the results of Wijnands et al. (1997a), we wished to combine the epoch 3 and epoch 4 data sets. Unfortunately, the tracks traced out in the CDs of epoch 3 and 4 are not the same, and two different splines had to be used for the S_z parameterization. Since the normal points for these splines were drawn by hand, the S_z scales for the epoch 3 and epoch 4 CDs were unlikely to be exactly the same. Therefore, we first transformed the S_z scale of epoch 4 to that of epoch 3. To accomplish this, we measured the frequency of either the HBO or NBO at several places along the Z track of epoch 3 and determined

TABLE 3
CHANNEL AND ENERGY BOUNDARIES OF THE SOFT AND HARD COLORS AND THE INTENSITY USED FOR THE SPECTRAL ANALYSIS

	Soft Color		Hard Color		Intensity	
Gain Epoch	Channels	keV	Channels	keV	Channels	keV
3.....	10–16/5–9	4.8–7.3/3.0–4.8	26–50/17–25	10.5–19.7/7.3–10.5	5–50	3.0–19.7
4.....	8–13/4–7	4.6–7.1/2.9–4.6	22–42/14–21	10.5–19.6/7.1–10.5	4–42	2.9–19.6

NOTE.—The channel numbers refer to the Standard 2 mode channels (1–129).

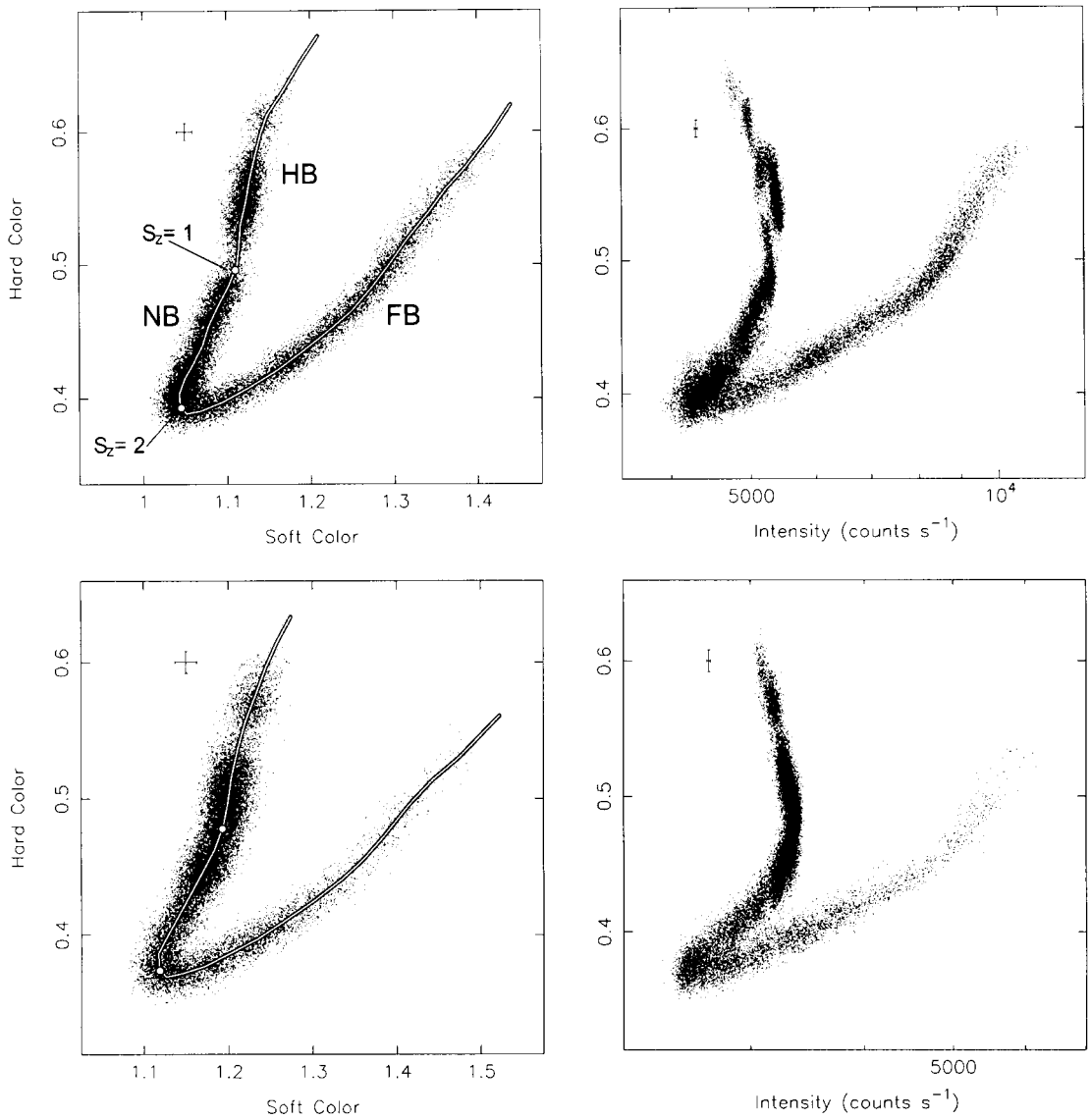

FIG. 1.—Color-color diagrams (*left column*) and hardness-intensity diagrams (*right column*) for the epoch 3 (*top*) and epoch 4 data (*bottom*). Each point represent a 16 s average. The splines and vertices (*white circles*) that were used for the S_z parameterization are shown, as are the typical error bars. See Table 3 for the energy bands used for the soft and hard color and intensity.

the S_z interval corresponding to the same frequency in the epoch 4 data. We found that $S_{z,\mathrm{epoch\,4}} = (0.06 \pm 0.04) + (1.005 \pm 0.018) S_{z,\mathrm{epoch\,3}}$, showing that, although the scales are the same (within the errors), a small shift is present. We subsequently scaled the S_z values of epoch 4 using the above expression. The above scaling method assumes that the HBO and NBO frequencies are strongly related to S_z. Previous studies of Z sources (see, e.g., Kuulkers et al. 1997; Wijnands et al. 1997a; Jonker et al. 2000a; Dieters & van der Klis 2000) as well as the fact that only little scatter was present around the linear relation seem to confirm this.

Power spectra were created from the data in modes with high time resolution ($\leq 2^{-13}$ s; see Table 2) using standard fast Fourier transform techniques (see van der Klis 1989 and references therein). The data were not background subtracted, and no dead-time corrections were applied prior to the Fourier transformations. We made power spectra in several energy bands, with several frequency resolutions and Nyquist frequencies. We finally settled on 0.0625–4096 Hz power spectra in the 5.1–60 keV (epoch 3) and 5.8–60 keV (epoch 4) bands, since the QPOs were most significantly detected in those bands (note that the source does not actually contribute significantly to the power spectra above ~40 keV; however, our data modes did not allow us to discard data above this energy). This choice of frequency range means that the properties of the VLFN, which dominates the power spectrum below 0.1 Hz, could not always be measured satisfactorily, but it does allow us to follow the power spectral evolution on timescales down to 16 s. Note that the power spectra of epoch 4 were produced in a slightly higher energy band than those of epoch 3. Because of the gain changes and the limited choice of energy channels, this was the best possible match.

The power spectra were selected on the basis of S_z, as determined from the CD. The S_z selections usually had a width of 0.1 and did not overlap—no power spectrum was represented in more than one S_z selection. Different widths were used in cases where the power spectrum changed rapidly as a function of S_z (narrower selections) or when the powers were weak (wider selections). All the power spectra

in a selection were averaged, and the resulting power spectrum was rms normalized according to a procedure described in van der Klis (1995b).

The properties of the power spectra were quantified by fitting functional forms to them. The low-frequency (0.0625–256 Hz) and high-frequency (100–4096 Hz) parts of the power spectrum were fitted separately. The high-frequency part was fitted with one or two Lorentzians (for the kHz QPO[s]) and with the function $P(\nu) = P_1 + P_2 \cos(2\pi\nu/\nu_N) + P_3 \cos(4\pi\nu/\nu_N)$ for the dead-time–modified Poisson level (Zhang 1995; Zhang et al. 1995); no separate term was used for the contribution of the very large events count rate since it was absorbed by this fit function. At low frequencies the noise that was present could not be fitted consistently, and varying combinations of functionals had to be used:

1. $S_z < 0.0$: a Lorentzian (LFN+VLFN),
2. $S_z = 0.0$–0.1: a cutoff power law (LFN+VLFN),
3. $S_z = 0.1$–1.4: a power law (VLFN) and a cutoff power law (LFN),
4. $S_z = 1.4$–1.6: a power law (VLFN) and a Lorentzian (LFN+NBO),
5. $S_z = 1.6$–5.0: a power law (VLFN) and a Lorentzian (LFN), and
6. $S_z > 5.0$: a power law (VLFN).

The expression for a power law is $P(\nu) \propto \nu^{-\alpha}$, that for a cutoff power law is $P(\nu) \propto \nu^{-\alpha} e^{-\nu/\nu_{\rm cut}}$ (where $\nu_{\rm cut}$ is the cutoff frequency), and that for a Lorentzian $P(\nu) \propto 1/[(\nu - \nu_c)^2 + (\mathrm{FWHM}/2)^2]$ (where ν_c is the centroid frequency and FWHM is the full width at half-maximum). The HBO, its second harmonic, and the NBO/FBO were each fitted with a Lorentzian. Below the HBO, at about half its frequency, a broad bump was present that was also fitted with a Lorentzian, whose frequency was sometimes fixed to zero. At low frequencies the dead-time–modified Poisson level was fitted with a constant. An example of a fit to a power spectrum ($S_z = 0.4$–0.5), displaying the contribution of the several components, is shown in Figure 4.

Note that changes in the fit function, such as using a cutoff power law instead of a Lorentzian or adding an extra component, may lead to minor changes in the values of other parameters. Errors on the fit parameters were determined using $\Delta\chi^2 = 1$. Upper limits were determined by fixing some or all of the parameters of a component, except the rms amplitude, to values similar to those obtained in the closest S_z selection where it was found to be significant, leaving all other fit parameters free, and using $\Delta\chi^2 = 2.71$ (95% confidence).

A study of the energy dependence and time lag properties of the QPOs and noise components will be presented elsewhere.

3. RESULTS

3.1. *Broadband Spectral Behavior*

The CDs and HIDs of both epochs are shown in Figure 1. In both CDs the HB/NB vertex is not well defined, since the HB is almost a continuation of the NB. This is mainly due to the relatively high energies that we chose for our soft color (see § 2). At lower energies the turnover is much clearer. In Figure 2 we show the count rate in several energy bands as a function of S_z, for epoch 4. It shows that the HB/NB vertex in the HID is entirely due to the count rates at low energies. At high energies the HB is a perfect continuation of the NB and no vertex is present.

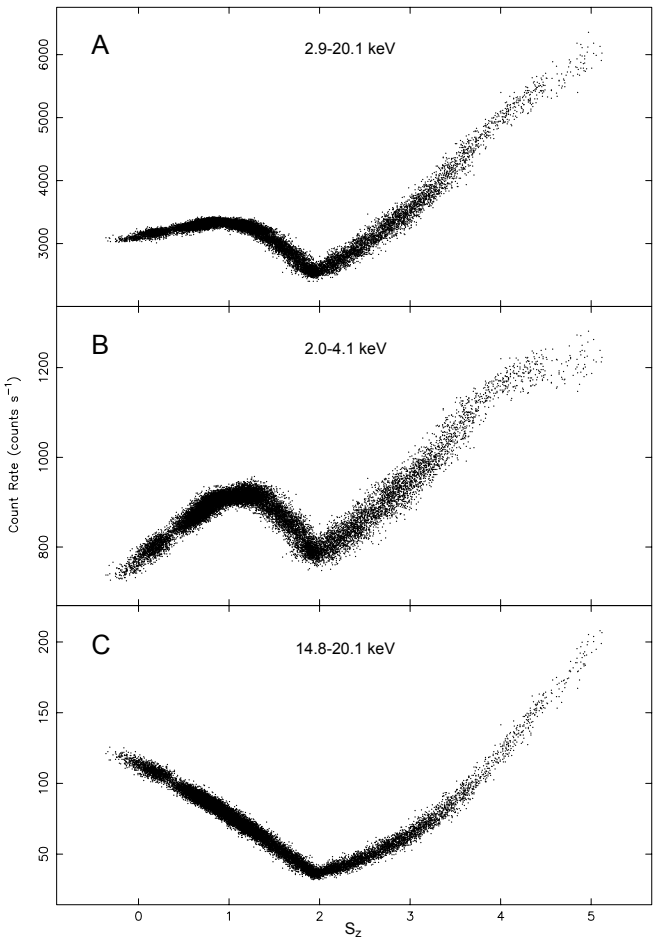

FIG. 2.—Count rate in three energy bands as a function of S_z (epoch 4 data only). The HB/NB vertex in the 2.9–20.1 keV band (*a*) is caused by the contribution from the low energies (*b*). This vertex does not show up at high energies (*c*).

In the HID of epoch 3, the Z track appears to be segmented, which was already noted by Wijnands et al. (1997a). Although no corrections for the slow detector aging processes were applied to the intensity in this HID, we note that a quick look showed that they would only have made the segmentation more apparent. The shifts in the HID might be due to the secular motion that has been observed in other Z sources. The shifts, of up to ~5% in intensity, do not show up in the CD. This is because colors are ratios of intensities and are therefore not very sensitive to overall intensity changes; exactly for this reason, CDs are preferable over HIDs for our purpose. Moreover, the width of the tracks in the CD is about 5%, so changes smaller than this are hard to observe.

The bottom panel of Figure 3 shows the distribution of the time spent by the source in each part of the Z track. The source spent 28% of the time on the HB ($S_z \leq 1$), 44.2% on the NB ($1 < S_z \leq 2$), and 27.8% on the FB ($S_z > 2$). The average speed along the Z track as a function of S_z ($\langle V_z \rangle$) is shown in the top panel of Figure 3. The speed at a given $S_z(i)$ is defined as $V_z(i) = |S_z(i+1) - S_z(i-1)|/32$ (see also Wijnands et al. 1997b), where i is used to number the points in order of time. As expected, the $\langle V_z \rangle$ increases considerably when the source enters the FB, but also at the top

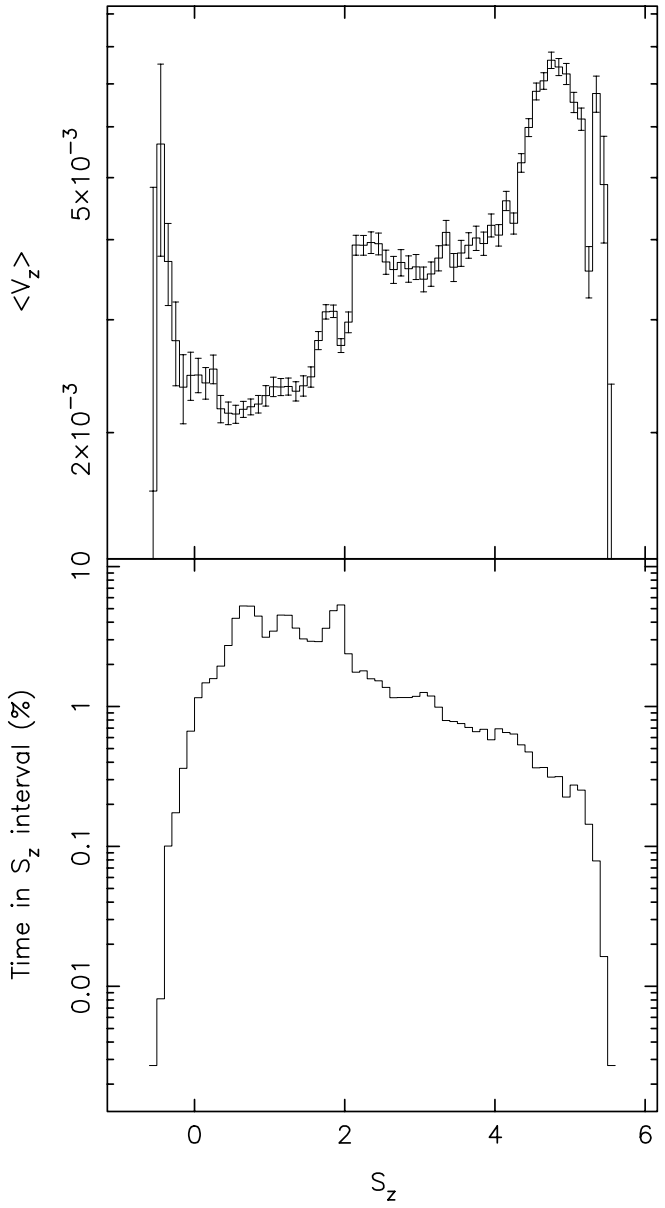

FIG. 3.—*Top*: Average speed along the Z track ($\langle V_z \rangle$). *Bottom*: Percentage of the time spent in each S_z interval as a function of S_z.

of the HB ($S_z < 0.5$). Combined with the small amount of time spent in the upper HB, we can conclude that the source reaches S_z values this low only in brief, quick dashes.

For a more detailed analysis of the spectral changes as a function of the position along the Z track in GX 17+2, we refer to K. O'Brien et al. (2002, in preparation).

3.2. *Power Spectra*

3.2.1. *Low-Frequency QPOs and Noise Components*

Figure 5 shows the low-frequency part (0.0625–256 Hz) of the power spectrum for nine different S_z selections. The power spectra shown in Figure 5 are selected from epoch 3 and epoch 4 and are therefore a combination of 5.1–60 keV and 5.8–60 keV data. The percentage of epoch 3 and epoch 4 data varies between the S_z selections. The contribution of epoch 3 data is highest at the extremes of the S_z range, reaching 100%, and gradually decreases from both ends to ~10% around $S_z = 1$.

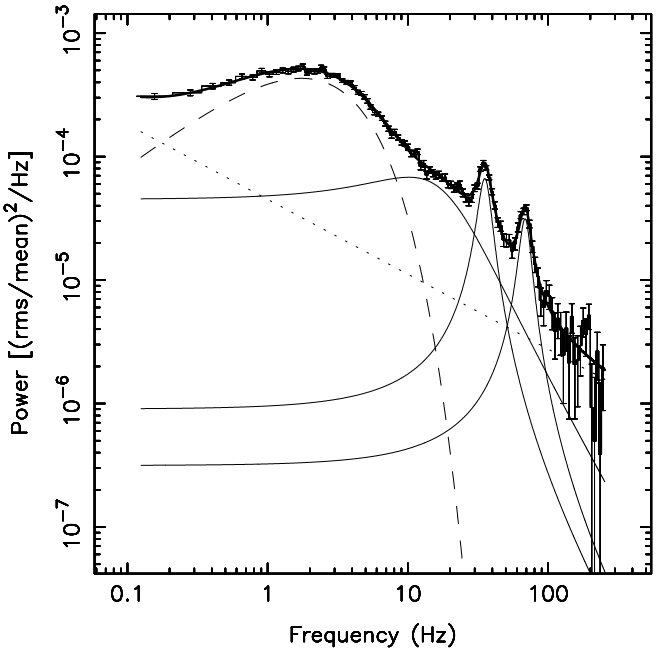

FIG. 4.—Example of a fit to the $S_z = 0.4$–0.5 power spectrum, showing the relative contribution of the individual components. The combined fit is represented by the thick solid line, the three Lorentzians/QPOs by the thin solid lines, the cutoff power law/LFN by the dashed line, and the power law/VLFN by the dotted line. The Poisson level was subtracted. The reduced χ^2 of this fit was 1.03 for 204 degrees of freedom.

Several components can be seen, which change in strength and shape as a function of S_z. The different components are identified in Figure 5 (see also Fig. 4), and the S_z ranges in which they were detected are given in Table 4. The component identified as the subharmonic of the HBO is rather broad and does not have the appearance of a QPO. However, based on the frequency ratios (see below) it is referred to as the HBO subharmonic.

Some difficulties were experienced while fitting the low-frequency part of the power spectrum between $S_z = 1.4$ and $S_z = 1.6$, where probably two or more components with similar frequencies were simultaneously present. Above $S_z = 1.4$ the NBO appeared, as a broad feature on top of the LFN. We were not able to distinguish the two components and decided to fit them together with a single Lorentzian. The fit values are not used in figures and tables, since they do not represent any of the individual components. Above $S_z = 1.6$, the NBO and LFN could be distinguished more easily. The fit function used for the LFN, which was underlying the NBO, was changed to a Lorentzian to be more consistent with fits at higher S_z (fits with a cutoff power law gave equally good $\chi^2_{\rm red}$ at this S_z).

In the following sections the results for each of the components will be presented.

3.2.2. *HBO*

The HBO was detected between $S_z = -0.6$ and $S_z = 2.1$ and its second harmonic between $S_z = -0.6$ and $S_z = 1.0$. The second and third columns of Figure 6 show their rms amplitudes, FWHMs, and frequencies as a function of S_z (see also Table 5). The frequency of the HBO increased from 21.3 Hz at $S_z = -0.43$ to 60.3 Hz at $S_z = 1.45$ and then

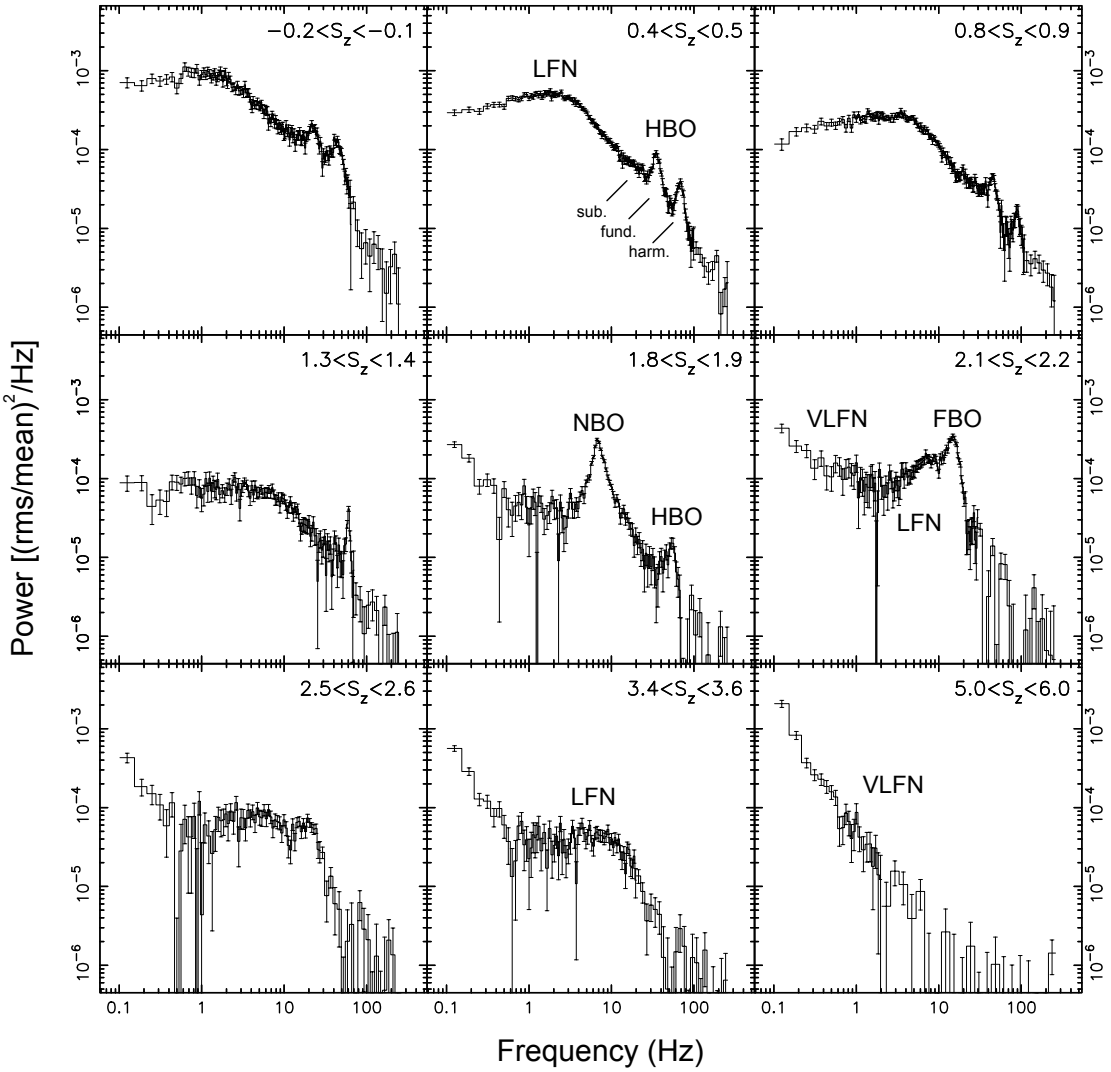

FIG. 5.—Power spectra (0.0625–256 Hz) for nine different S_z selections. The Poisson level was subtracted for all power spectra. The most important power spectral features are indicated.

decreased to 48.2 Hz at $S_z = 2.04$. The second harmonic of the HBO had a frequency that was on average 1.941 ± 0.007 times that of the first harmonic, which is significantly different from the expected value of 2. An explanation for this discrepancy is proposed in § 4.1.2. Between $S_z = -0.6$ and $S_z = 1.0$, both the HBO and its second harmonic decreased in strength, with the decrease of the second harmonic occurring somewhat faster than that of the HBO. In that same S_z interval, the FWHM of the HBO and its second harmonic were fairly constant (showing a slight increase), although considerable scatter was present around the average values (which were, respectively, 7.9 ± 0.3 Hz and 14.4 ± 0.6 Hz). The Q-values of the HBO and its harmonic are shown in Figure 7. In the S_z range where both were detected, their Q-values were consistent with each other. When the second harmonic was not significantly detected anymore ($S_z > 1.0$), the rms amplitude and the FWHM of the HBO both decreased from, respectively, $2.45\% \pm 0.08\%$ and 9.7 ± 0.7 Hz ($S_z = 0.5$–1.0) to $1.48\% \pm 0.06\%$ and 5.1 ± 0.4 Hz ($S_z = 1.0$–1.5). Between $S_z = 1.0$ and $S_z = 1.5$, the relation between the S_z and the HBO frequency started to flatten. Above $S_z = 1.5$, the frequency of the HBO clearly dropped, initially quite abruptly and later on more smoothly. This frequency drop coincided with an increase in the FWHM to 15.7 ± 1.5 ($S_z = 1.5$–2.1); the rms amplitude showed a small increase to $2.1\% \pm 0.1\%$ ($S_z = 1.76$), followed by a decrease to $1.2\% \pm 0.2\%$ ($S_z = 2.04$).

TABLE 4
THE NINE DIFFERENT COMPONENTS IN THE COMBINED EPOCH 3/EPOCH 4 POWER SPECTRA AND THE S_z RANGES IN WHICH THEY WERE DETECTED

Component	S_z Range
LFN	−0.6 to 5.0
HBO (fundamental)	−0.6 to 2.1
HBO (second harmonic)	−0.6 to 1.0
HBO (subharmonic)	−0.6 to 1.3
Upper kHz QPO	−0.3 to 1.7
VLFN	0.3 to 5.5
Lower kHz QPO	0.5 to 1.5
NBO	1.6 to 2.1
FBO	2.0 to 2.7

NOTE.—The components are listed in order of S_z appearance.

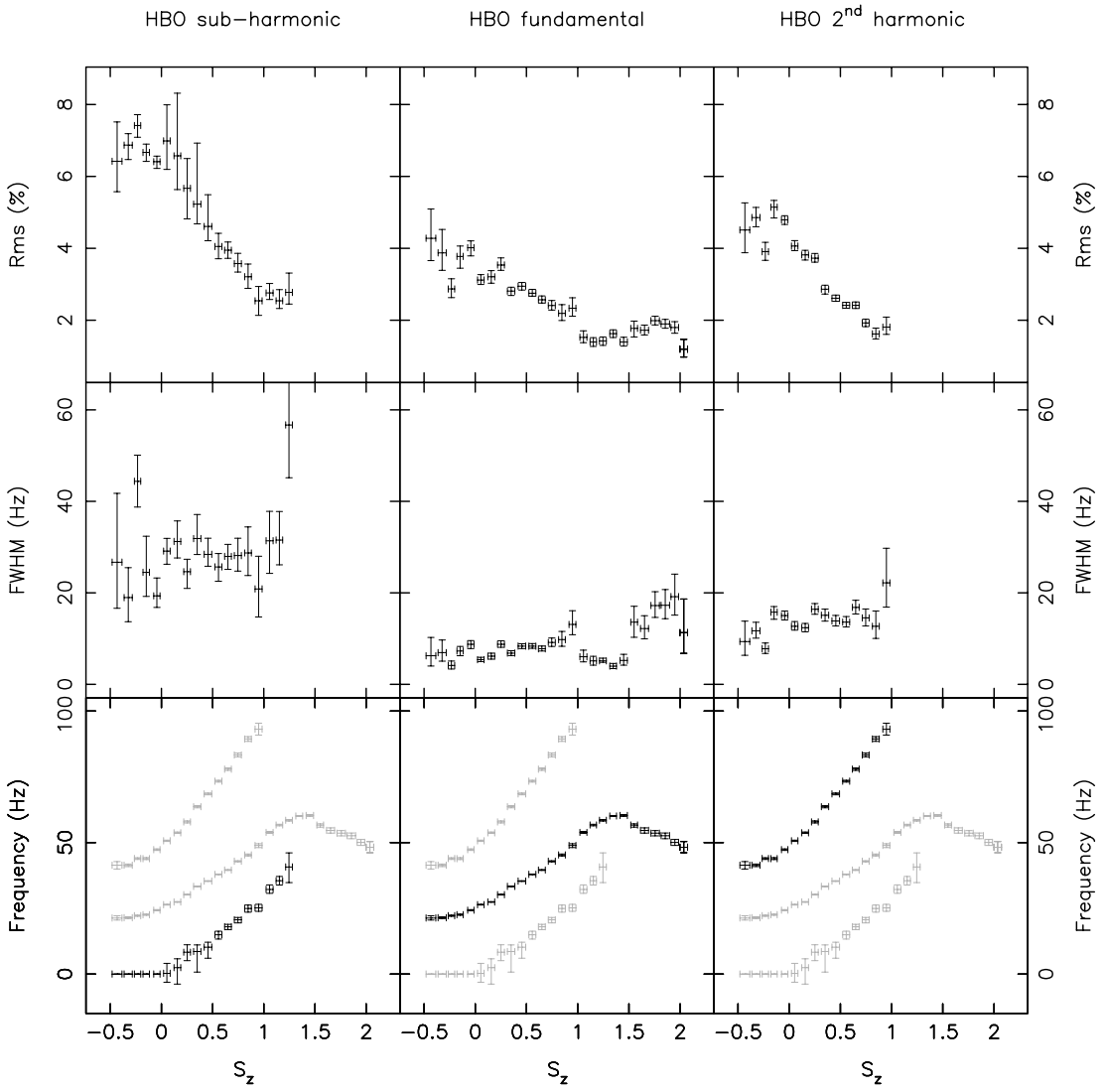

FIG. 6.—Properties of the HBO (*middle column*), its second harmonic (*right column*), and subharmonic (*left column*) as a function of S_z. For reasons of comparison the frequency of the other two QPOs (*gray*) are also plotted in the frequency plot of each QPO.

Underlying the HBO and its second harmonic, but with a central frequency lower than that of the HBO, we found a broad feature that was also fitted with a Lorentzian. It was significantly detected between $S_z = -0.6$ and $S_z = 1.3$. The properties of the broad feature are shown in the first column of Figure 6 (see also Table 5). Below $S_z = 0$ the frequency of the Lorentzian was fixed to zero. Between $S_z = 0.5$ and $S_z = 1.5$, the frequency of the broad feature is on average 0.539 ± 0.015 times that of the HBO. This could mean that the broad feature is the subharmonic of the HBO, certainly when one takes into account that the frequency of a broad feature is rather sensitive to the shape of the continuum. Whereas the rms amplitude and the frequency of the subharmonic both change strongly with S_z, the FWHM remains more or less constant, with an average value of 29.5 ± 1.5 Hz.

3.2.3. *NBO and FBO*

The NBO and FBO were detected between $S_z = 1.6$ and $S_z = 2.7$. The fit results for the NBO/FBO are shown in Figure 8 (see also Table 5). Below $S_z = 2.1$, the NBO (represented by the filled circles in Fig. 8) had a fairly constant frequency, with values between 6.3 and 7.0 Hz. Its rms amplitude increased from 1.7% to 3.2%, and the FWHM was approximately ~2.1 or ~3.8. In the $S_z = 2.0$–2.1 selection, both the NBO and FBO were present. This is likely an artifact of the S_z selection method, since a careful inspection of dynamical power spectra showed no evidence for simultaneous presence of both QPOs. It is interesting to note, though, that in the $S_z = 2.0$–2.1 selection the frequency of the FBO was 2.0 ± 0.1 times that of the NBO, which could mean that the NBO and FBO are harmonically related (however, see below). The FBO increased in frequency from 13.9 Hz ($S_z = 2.04$) to 23.1 Hz ($S_z = 2.65$), while its FWHM increased from ~5 to ~13 Hz. The rms amplitude of the FBO initially continued the trend of the NBO rms amplitude; it increased from 2.8% ($S_z = 2.04$) to 5.6% ($S_z = 2.23$), but then decreased to 1.8% ($S_z = 2.65$).

To study the transitions between the NBO and FBO more carefully, we inspected all dynamical power spectra of observations with S_z values around 2. Although no clear transitions were found, mainly because of the limited quality of the dynamical power spectra, we did in some cases see

TABLE 5

FIT RESULTS FOR THE LOW-FREQUENCY QPOS

	HBO FUNDAMENTAL			HBO SECOND HARMONIC			HBO SUBHARMONIC			NBO		
S_z	rms[a] (%)	FWHM (Hz)	Frequency (Hz)	rms[a] (%)	FWHM (Hz)	Frequency (Hz)	rms[b] (%)	FWHM (Hz)	Frequency (Hz)	rms[b] (%)	FWHM (Hz)	Frequency (Hz)
-0.43 ± 0.05	4.3 ± 0.7	6^{+4}_{-2}	21.3 ± 0.8	4.5 ± 0.7	9^{+4}_{-3}	41.4 ± 1.4	6.4 ± 1.0	27^{+15}_{-10}	0 (fixed)	...	...	...
-0.32 ± 0.04	3.9 ± 0.6	$6.9^{+2.8}_{-1.9}$	21.4 ± 0.4	4.9 ± 0.3	11.7 ± 1.7	41.4 ± 0.5	6.9 ± 0.4	19 ± 6	0 (fixed)	...	...	...
-0.23 ± 0.03	2.9 ± 0.3	4.1 ± 0.9	22.2 ± 0.2	3.9 ± 0.2	7.8 ± 1.1	43.9 ± 0.3	7.4 ± 0.3	44 ± 6	0 (fixed)	...	...	...
-0.15 ± 0.03	3.8 ± 0.3	7.3 ± 1.0	22.6 ± 0.3	$5.14^{+0.19}_{-0.30}$	15.8 ± 1.4	43.9 ± 0.4	6.7 ± 0.2	24^{+8}_{-5}	0 (fixed)	...	...	...
-0.04 ± 0.03	4.02 ± 0.20	8.7 ± 0.9	24.3 ± 0.2	4.79 ± 0.12	15.0 ± 1.0	47.3 ± 0.3	6.41 ± 0.17	19^{+4}_{-3}	0 (fixed)	...	...	...
0.05 ± 0.03	3.12 ± 0.14	5.4 ± 0.5	26.39 ± 0.13	4.06 ± 0.14	12.7 ± 0.9	50.7 ± 0.2	7.0 ± 0.9	29 ± 3	0 ± 4	...	...	...
0.16 ± 0.03	3.21 ± 0.18	6.1 ± 0.6	27.42 ± 0.14	3.82 ± 0.13	12.4 ± 0.9	53.7 ± 0.3	$6.6^{+1.7}_{-0.9}$	31 ± 4	2^{+3}_{-6}	...	...	...
0.25 ± 0.03	3.54 ± 0.17	8.8 ± 0.7	30.20 ± 0.18	3.73 ± 0.12	16.4 ± 1.2	57.9 ± 0.4	5.7 ± 0.8	25 ± 3	8 ± 3	...	...	...
0.35 ± 0.04	2.81 ± 0.11	6.8 ± 0.5	33.33 ± 0.15	2.86 ± 0.12	15.0 ± 1.3	63.6 ± 0.4	$5.2^{+1.7}_{-0.5}$	32^{+5}_{-3}	9^{+2}_{-8}	...	...	...
0.46 ± 0.04	2.95 ± 0.11	8.3 ± 0.5	35.35 ± 0.15	2.61 ± 0.09	13.9 ± 1.2	68.5 ± 0.4	$4.6^{+0.9}_{-0.4}$	28 ± 3	$10^{+1.8}_{-4.2}$	...	...	...
0.56 ± 0.03	2.75 ± 0.09	8.3 ± 0.5	37.91 ± 0.14	2.41 ± 0.08	13.6 ± 1.1	73.4 ± 0.3	4.1 ± 0.4	26 ± 3	15.0 ± 1.5	...	...	...
0.65 ± 0.03	2.57 ± 0.10	7.8 ± 0.6	39.56 ± 0.14	2.42 ± 0.09	16.8 ± 1.5	77.9 ± 0.5	3.9 ± 0.2	28 ± 3	18.0 ± 1.0	...	...	...
0.75 ± 0.03	2.41 ± 0.13	9.1 ± 0.9	42.9 ± 0.2	1.92 ± 0.11	14.5 ± 1.9	83.3 ± 0.7	3.6 ± 0.3	28 ± 4	20.6 ± 1.0	...	...	...
0.85 ± 0.03	2.2 ± 0.2	9.8 ± 1.6	45.3 ± 0.4	1.62 ± 0.15	13 ± 3	89.4 ± 0.9	3.2 ± 0.3	29 ± 5	24.9 ± 1.4	...	...	...
0.95 ± 0.03	2.3 ± 0.3	$13. \pm 3$	48.9 ± 0.7	1.8 ± 0.2	22^{+8}_{-5}	93 ± 2	2.5 ± 0.4	21 ± 7	25.2 ± 1.3	...	...	...
1.06 ± 0.03	1.52 ± 0.17	6.0 ± 1.3	53.9 ± 0.4	1.09 ± 0.15	15 (fixed)	107 (fixed)	$2.76^{+0.26}_{-0.19}$	31 ± 7	32.2 ± 1.6	...	...	...
1.15 ± 0.03	1.40 ± 0.12	5.1 ± 1.0	56.7 ± 0.3	<0.7	15 (fixed)	113 (fixed)	$2.5^{+0.3}_{-0.2}$	32 ± 6	35.5 ± 1.6	...	...	...
1.25 ± 0.03	1.42 ± 0.12	$5.1^{+0.6}_{-0.3}$	58.5 ± 0.3	...	...	...	$2.8^{+0.5}_{-0.3}$	57^{+17}_{-12}	41 ± 6	...	...	...
1.35 ± 0.03	1.63 ± 0.11	4.0 ± 0.6	60.11 ± 0.17	...	...	...	<2.5	21 ± 14	43 ± 3	...	...	...
1.45 ± 0.04	1.40 ± 0.12	5.2 ± 1.2	60.3 ± 0.3	...	...	...	...	...	...	...	...	...
1.55 ± 0.03	1.8 ± 0.2	14 ± 3	$56.7^{+0.5}_{-0.8}$	...	...	...	...	...	...	...	...	...
1.65 ± 0.04	1.72 ± 0.14	12 ± 3	54.6 ± 1.0	...	...	...	...	...	...	1.7 ± 0.2	3.8 ± 0.7	6.33 ± 0.16
1.76 ± 0.04	1.99 ± 0.12	17 ± 3	53.6 ± 1.0	...	...	...	...	...	...	2.07 ± 0.11	2.08 ± 0.20	6.82 ± 0.04
1.86 ± 0.04	1.90 ± 0.12	17 ± 3	52.6 ± 1.1	...	...	...	...	...	...	2.89 ± 0.08	2.13 ± 0.11	6.91 ± 0.03
1.95 ± 0.04	1.80 ± 0.16	19 ± 4	50.1 ± 1.2	...	...	...	...	...	...	2.94 ± 0.12	2.11 ± 0.13	6.96 ± 0.02
2.04 ± 0.04	1.2 ± 0.2	11^{+7}_{-5}	48.2 ± 2	...	...	...	...	...	...	3.2 ± 0.2	3.7 ± 0.4	6.86 ± 0.10
	...	...	...	...	...	...	...	...	...	2.8 ± 0.8	$5.4^{+0.6}_{-1.4}$	$13.9^{+0.6}_{-0.4}$
2.13 ± 0.05	<1.2	9 (fixed)	46 (fixed)	...	...	...	...	...	...	4.93 ± 0.11	5.1 ± 0.2	14.78 ± 0.08
2.23 ± 0.06	...	...	...	...	...	...	...	...	...	5.60 ± 0.07	6.4 ± 0.18	15.44 ± 0.06
2.34 ± 0.05	...	...	...	...	...	...	...	...	...	5.28 ± 0.11	8.1 ± 0.3	16.75 ± 0.12
2.45 ± 0.05	...	...	...	...	...	...	...	...	...	4.37 ± 0.17	10.3 ± 0.7	18.2 ± 0.2
2.54 ± 0.04	...	...	...	...	...	...	...	...	...	3.36 ± 0.20	13.6 ± 1.6	19.7 ± 0.6
2.65 ± 0.04	...	...	...	...	...	...	...	...	...	1.8 ± 0.4	8 ± 4	23.1 ± 0.9
2.75 ± 0.04	...	...	...	...	...	...	...	...	...	<1.8	10 (fixed)	25 (fixed)

[a] Integrated between $-\infty$ Hz and $+\infty$ Hz.

[b] Integrated between 0 Hz and $+\infty$ Hz, because of low Q-values.

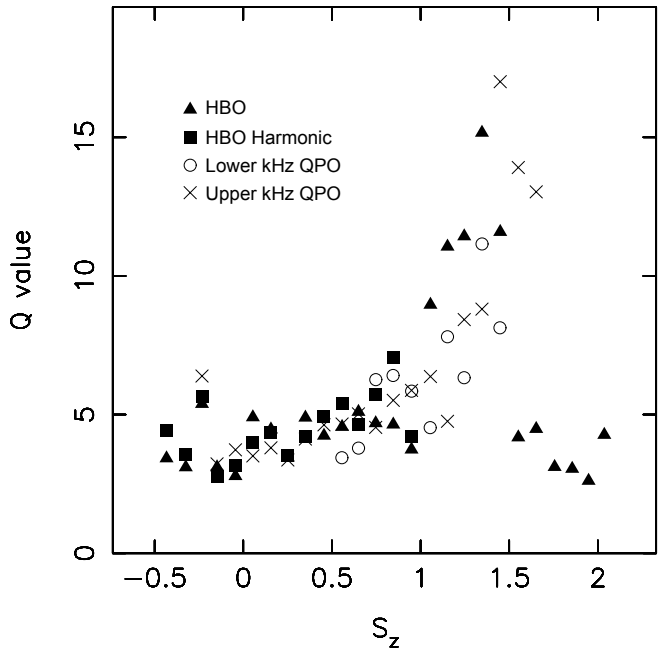

FIG. 7.—*Q*-values (frequency/FWHM) of the HBO, its harmonic, and the two kHz QPOs as a function of S_z. For reasons of clarity the error bars, which at a given S_z in general overlapped, were omitted.

QPOs with intermediate frequencies (~10 Hz), suggesting that the frequency does not jump directly from ~7 to ~14 Hz. Fitting the power spectra in consecutive time intervals (longer than 16 s) rather than inspecting dynamical power spectra with the eye will probably lead to more conclusive results but is beyond the scope of the current paper. The timescales on which the NBO/FBO frequency changed from ~7 to ~14 Hz and back were as short as a few tens of seconds.

We also studied the behavior of the NBO/FBO during two long type I X-ray bursts. The first one started on 1998 November 18 at 08:51:26 UTC, the second one on 1999 October 10 at 09:10:47 UTC. Their exponential decay times were, respectively, 189 ± 2 s and 144 ± 2 s (Kuulkers et al. 2001). Both bursts occurred near the NB/FB vertex, and in the power spectra of their respective observations, the NBO/FBO is clearly detected. No other QPOs were detected in the power spectra of these bursts. Figure 9 shows the dynamical power spectra of both bursts, together with their 2–60 keV light curves. During the brightest part of the bursts the NBO/FBO seemed to disappear. Apparently, the burst flux was not modulated at the NBO/FBO frequencies with the same amplitude as the persistent flux. To quantify this, we determined upper limits on the NBO/FBO strength and compared those with the values outside the bursts. The results are shown in Table 6. Clearly, during the brightest part of the bursts the rms amplitude of the NBO/FBO was significantly weaker, not only as a fraction of the total flux but also in absolute terms (and hence as a fraction of the persistent flux, if the persistent emission is assumed to continue during the bursts). These measurements constitute the first determination of the effect of X-ray bursts on the NBO/FBO. The fact that the bursts suppress the QPO can have important consequences for our understanding of its formation mechanism (see § 4.1.6).

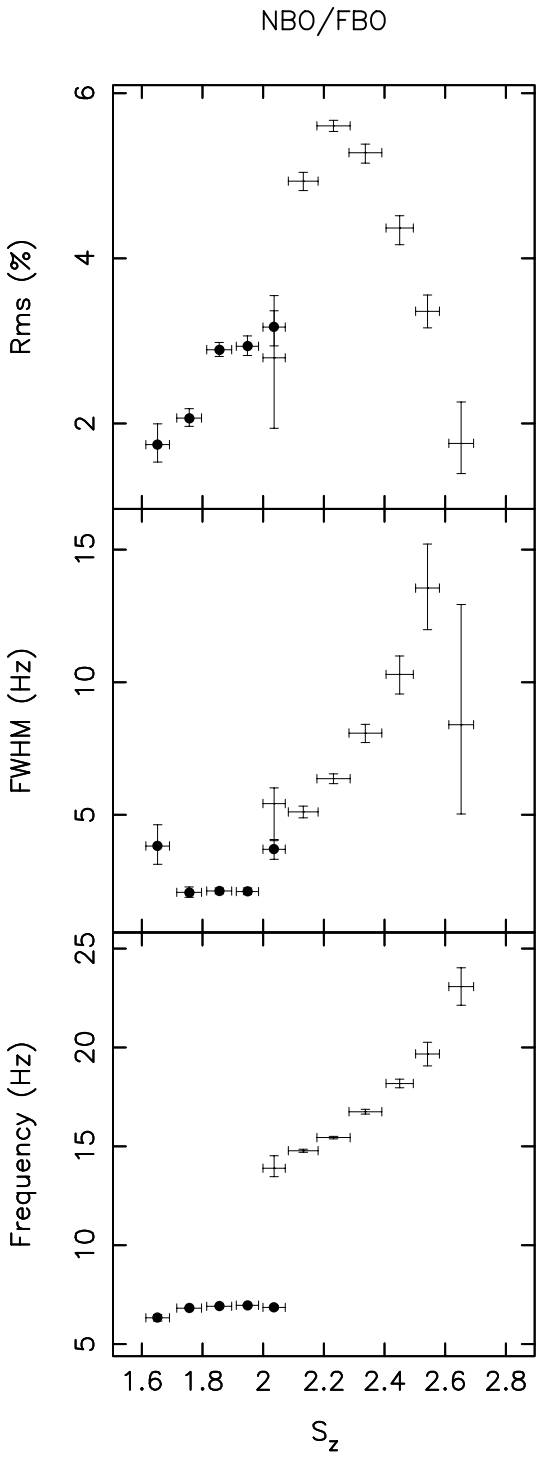

FIG. 8.—Properties of the NBO (*filled circles*) and FBO as a function S_z.

3.2.4. *Noise Components: LFN and VLFN*

LFN was detected between $S_z = -0.6$ and $S_z = 5.0$. As mentioned before, the appearance of the NBO around $S_z = 1.4$ kept us from putting firm constraints on the LFN parameters between $S_z = 1.4$ and $S_z = 1.6$. The fit results for the LFN are shown in Figure 10 (see also Table 7) in two separate columns: one for the fits with a cutoff power-law fit ($S_z = 0.0$–1.4) and one for the fits with a Lorentzian ($S_z < 0.0$ and $S_z = 1.6$–5.0). The strength of the LFN was

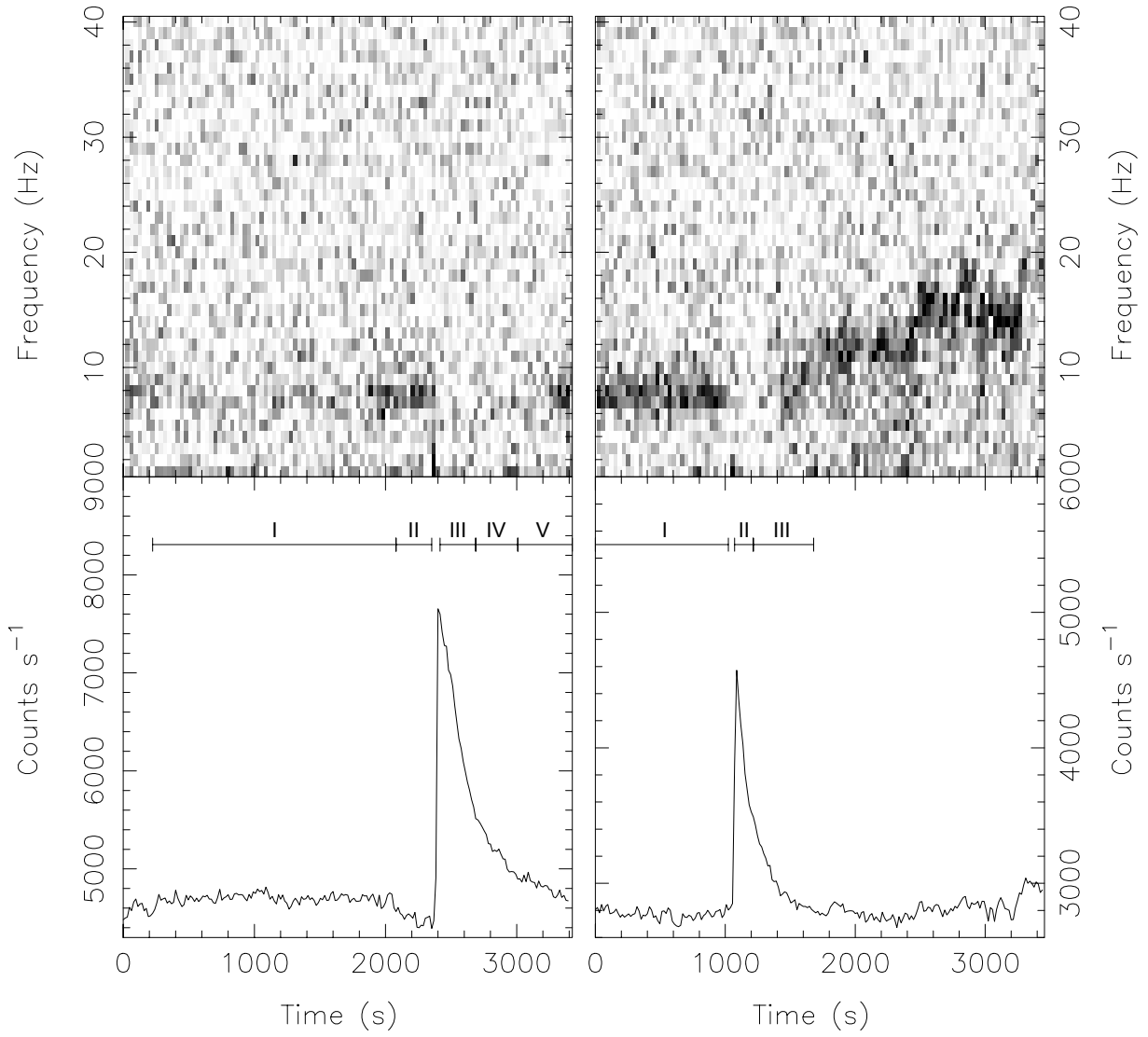

FIG. 9.—Dynamical power spectra *(top panels)* and light curves in the 2–60 keV band *(bottom panels)* of the two type I X-ray bursts in which we studied the behavior of the NBO/FBO. The 1998 November burst is shown on the left (five PCUs) and the 1999 October burst on the right (three PCUs). The intervals in which we measured the NBO/FBO are indicated by Roman numerals (see Table 6). The shades of gray in the dynamical power spectra represent the Leahy power, with darker shades indicating higher powers.

TABLE 6
THE PROPERTIES OF THE NBO/FBO DURING THE TWO BURSTS SHOWN IN FIGURE 9

Interval	Count Rate (counts s^{-1})	Fractional rms (%)	Absolute rms (counts s^{-1})
1998 Nov (I).....	2811	2.58 ± 0.19	72.5 ± 5.3
1998 Nov (II)	2648	3.2 ± 0.3	85 ± 8
1998 Nov (III)...	4568	<0.71	<32.4
1998 Nov (IV) ...	3232	<2.1	<68
1998 Nov (V).....	2833	3.3 ± 0.2	93 ± 6
1999 Oct (I).....	1742	5.56 ± 0.17	96.9 ± 3.0
1999 Oct (II).....	2616	<1.57	<41.1
1999 Oct (III)	1847	4.3 ± 0.4	79 ± 7

NOTES.—The intervals given in first column can also be found in Figure 9. The upper limits in the last two columns are 95% confidence. The count rates are in the 5.1–60 keV (1998 November, five PCUs) and 5.8–60 keV (1999 October, three PCUs) bands.

in both cases defined as the integrated power spectral density between 1 and 100 Hz. We note that below $S_z = 0.1$ the VLFN was not fitted separately from the LFN. An inspection of 1/256–4096 Hz power spectra below $S_z = 0.1$ showed that a weak power-law component was present at frequencies below 0.1 Hz. This component was probably VLFN; its power in the 1–100 Hz range was much smaller than that of the LFN, so although some VLFN power was absorbed by the LFN, this did not affect the LFN rms amplitudes significantly. The strength of the LFN changed considerably as a function of S_z. It showed a narrow peak between $S_z = -0.6$ and $S_z = 0.2$ of ~5% rms. Between $S_z = 0.2$ and $S_z = 1.7$, it gradually decreased from ~4.5% rms to ~2.5% rms. Another decrease was observed between $S_z = 2.7$ and $S_z = 5.0$, from ~3.8% rms to ~0.9% rms. The behavior between $S_z = 1.7$ and $S_z = 2.7$ was quite erratic, probably because of interactions with the fit functions of NBO and FBO.

The centroid frequency of a Lorentzian and the cutoff frequency of a cutoff power law cannot be directly compared.

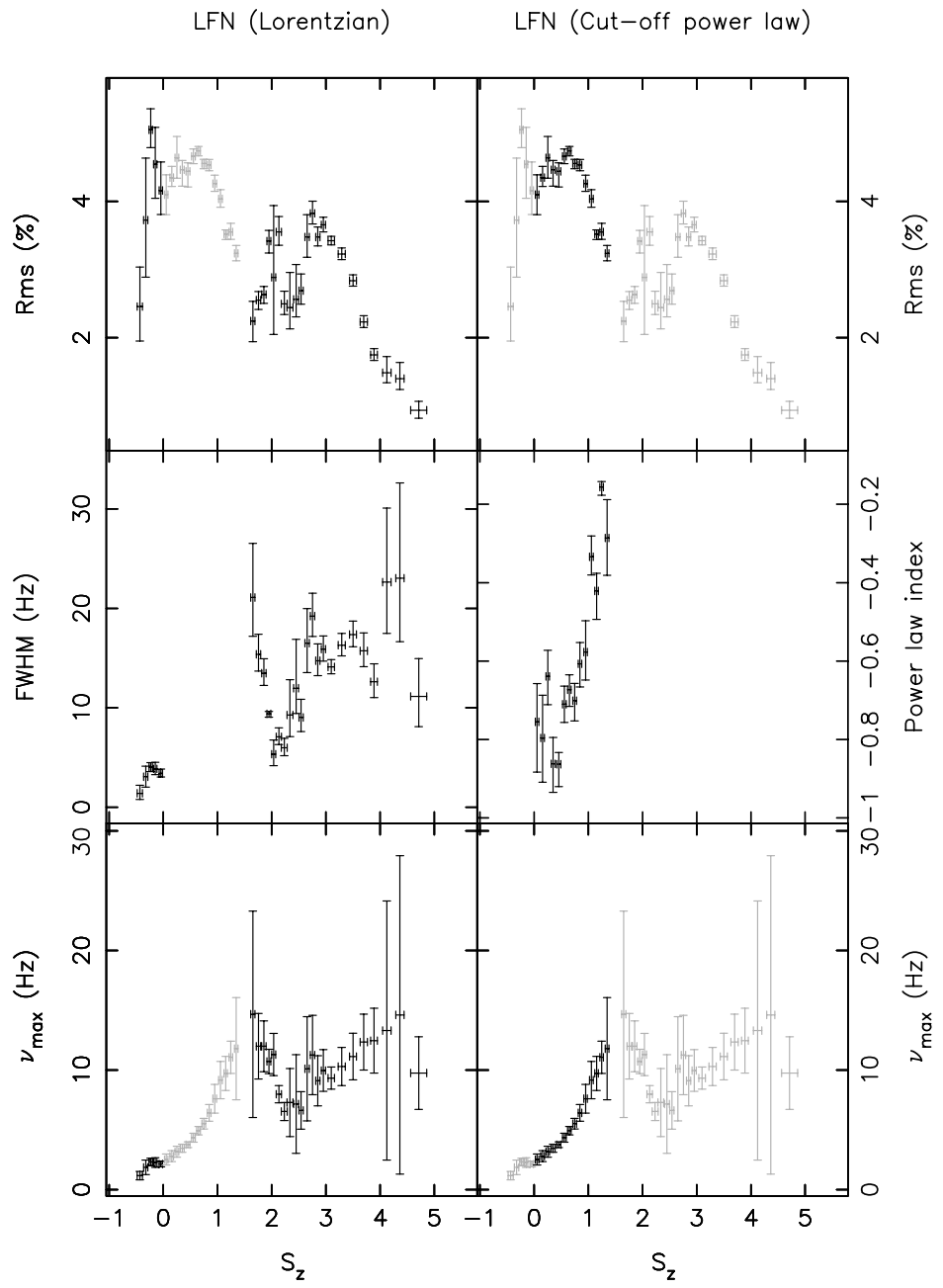

FIG. 10.—LFN properties as function of S_z. The left column shows the results for the fits with a Lorentzian, the right column those for fits with a cutoff power law. In both cases the rms amplitude is the integrated power in the 1–100 Hz range. The term ν_{max} is the frequency at which most of the power is concentrated (see text for the expressions for ν_{max}). For reasons of comparison we also plotted the values of the other fit function (*gray*) in the panels for the rms amplitude and ν_{max}.

Since we wanted to see how the typical frequency of the LFN evolved with S_z, we chose to plot ν_{max}, which is the maximum in a $\nu P(\nu)$ plot and the frequency at which most of the power is concentrated per logarithmic frequency interval (T. Belloni, D. Psaltis, & M. van der Klis 2002, in preparation). For a Lorentzian, ν_{max} is $[\nu_c^2 + (\mathrm{FWHM}/2)^2]^{1/2}$, and for a cutoff power law ν_{max} is $(1-\alpha)\nu_{cut}$ (see § 2 for analytical expressions for a Lorentzian and cutoff power law). As can be seen from Figure 10, between $S_z = -0.6$ and $S_z = 1.7$, ν_{max} smoothly increased from ~1.2 to ~14.7 Hz. Above $S_z = 1.7$, the errors on ν_{max} were larger and the behavior was less clear. Between $S_z = 1.7$ and $S_z = 2.3$, ν_{max} decreased to ~6.5 Hz, and above $S_z = 2.3$ it increased again to ~15 Hz. We tested whether the change of the fit functions at $S_z = 0.0$ affected the values for ν_{max} and the other power spectral parameters by swapping the fit functions used below and above $S_z = 0.0$; no significant changes were found.

VLFN was detected over almost the whole S_z range. Although we started fitting the VLFN separately from the LFN only above $S_z = 0.1$ (in the 16 s power spectra), VLFN was present at frequencies below 0.1 Hz in the 256 s power spectra below $S_z = 0.1$. In the 16 s power spectra it was significantly detected only above $S_z = 0.3$. The fit results for the VLFN are shown in Figure 11 (see also Table 7). Between $S_z = 0.3$ and $S_z = 1.4$ the VLFN strength

TABLE 7

FIT RESULTS FOR THE NOISE COMPONENTS AT LOW FREQUENCIES

	VLFN		LFN (CUTOFF POWER LAW)			LFN (LORENTZIAN)		
S_z	rms[a] (%)	Index	rms[b] (%)	Index	Cutoff (Hz)	rms[b] (%)	FWHM (Hz)	Frequency (Hz)
-0.43 ± 0.05	...	...	...	...	...	2.5 ± 0.5	1.4 ± 0.7	0.9 ± 0.3
-0.32 ± 0.04	...	...	...	...	...	3.7 ± 0.9	3.1 ± 1.0	1.05 ± 0.19
-0.23 ± 0.03	...	...	...	...	...	5.0 ± 0.3	4.0 ± 0.4	1.15 ± 0.13
-40.15 ± 0.03	...	...	...	...	...	4.5 ± 0.5	3.9 ± 0.6	1.19 ± 0.09
-0.04 ± 0.03	...	...	...	...	...	4.2 ± 0.4	3.4 ± 0.4	1.30 ± 0.06
0.05 ± 0.03	...	...	4.1 ± 0.3	-0.76 ± 0.11	1.43 ± 0.15	...	...	...
0.16 ± 0.03	<0.9	0.6 (fixed)	4.35 ± 0.15	-0.80 ± 0.11	$1.56^{+0.16}_{-0.11}$	...	...	...
0.25 ± 0.03	<0.7	0.6 (fixed)	4.6 ± 0.3	-0.64 ± 0.07	1.93 ± 0.19	...	...	...
0.35 ± 0.04	0.86 ± 0.07	0.69 ± 0.04	$4.46^{+0.14}_{-0.24}$	-0.86 ± 0.07	$1.85^{+0.12}_{-0.08}$	...	...	...
0.46 ± 0.04	0.83 ± 0.06	0.61 ± 0.03	$4.44^{+0.13}_{-0.23}$	$-0.86^{+0.03}_{-0.06}$	$2.01^{+0.06}_{-0.12}$	...	...	...
0.56 ± 0.03	0.65 ± 0.06	0.66 ± 0.05	4.66 ± 0.11	-0.71 ± 0.05	2.54 ± 0.14	...	...	...
0.65 ± 0.03	0.65 ± 0.06	$0.85^{+0.15}_{-0.09}$	4.74 ± 0.07	-0.67 ± 0.04	2.94 ± 0.12	...	...	...
0.75 ± 0.03	0.74 ± 0.05	0.57 ± 0.03	4.55 ± 0.07	-0.70 ± 0.05	3.24 ± 0.14	...	...	...
0.85 ± 0.03	0.61 ± 0.08	0.47 ± 0.05	4.53 ± 0.08	-0.61 ± 0.06	4.0 ± 0.2	...	...	...
0.95 ± 0.03	0.67 ± 0.07	$0.64^{+0.09}_{-0.06}$	4.26 ± 0.12	-0.58 ± 0.08	4.8 ± 0.4	...	...	...
1.06 ± 0.03	<0.5	0.4 (fixed)	4.04 ± 0.13	-0.33 ± 0.05	6.9 ± 0.6	...	...	...
1.15 ± 0.03	0.60 ± 0.05	0.58 ± 0.04	3.52 ± 0.07	$-0.42^{+0.04}_{-0.07}$	6.8 ± 0.4	...	...	...
1.25 ± 0.03	<0.5	0.5 (fixed)	3.55 ± 0.12	$-0.156^{+0.014}_{-0.021}$	$9.6^{+0.4}_{-0.8}$	...	...	...
1.35 ± 0.03	0.43 ± 0.09	0.60 ± 0.15	3.24 ± 0.11	-0.29 ± 0.10	9.2 ± 1.2	...	...	...
1.45 ± 0.04	0.63 ± 0.04	$0.68^{+0.10}_{-0.06}$	...	...	...	...	...	...
1.55 ± 0.03	0.71 ± 0.04	0.54 ± 0.03	...	...	...	...	...	...
1.65 ± 0.04	0.62 ± 0.05	1.29 ± 0.19	...	...	...	2.2 ± 0.3	21 ± 5	10 ± 2
1.76 ± 0.04	0.62 ± 0.04	1.6 ± 0.2	...	...	...	2.55 ± 0.13	15.4 ± 1.8	9.2 ± 0.7
1.86 ± 0.04	0.70 ± 0.03	1.48 ± 0.14	...	...	...	2.63 ± 0.12	13.5 ± 1.3	9.9 ± 0.6
1.95 ± 0.04	0.82 ± 0.03	0.92 ± 0.10	...	...	...	3.42 ± 0.17	9.4 ± 0.3	9.6 ± 0.3
2.04 ± 0.04	1.34 ± 0.03	0.77 ± 0.03	...	...	...	2.9 ± 0.9	5.3 ± 1.3	11.0 ± 0.5
2.13 ± 0.05	1.03 ± 0.05	1.01 ± 0.11	...	...	...	3.6 ± 0.2	7.1 ± 0.8	7.1 ± 0.20
2.23 ± 0.06	0.85 ± 0.05	$0.86^{+0.11}_{-0.07}$	...	...	...	2.50 ± 0.17	6.0 ± 0.9	5.8 ± 0.2
2.34 ± 0.05	1.02 ± 0.08	$1.12^{+0.23}_{-0.16}$	...	...	...	$2.4^{+0.5}_{-0.3}$	9^{+4}_{-2}	5.6 ± 0.7
2.45 ± 0.05	0.52 ± 0.05	$3.93^{+2.2}_{-1.1}$	...	...	...	$2.6^{+0.5}_{-0.3}$	12^{+5}_{-3}	$3.9^{+0.7}_{-1.0}$
2.54 ± 0.04	0.67 ± 0.06	2.5 ± 0.4	...	...	...	2.7 ± 0.2	9.0 ± 1.6	4.8 ± 0.4
2.65 ± 0.04	0.66 ± 0.08	1.7 ± 0.4	...	...	...	3.5 ± 0.3	16 ± 3	5.8 ± 0.7
2.75 ± 0.04	0.59 ± 0.07	$2.8^{+0.9}_{-0.6}$	...	...	...	3.82 ± 0.17	19 ± 3	5.9 ± 0.4
2.85 ± 0.04	0.46 ± 0.06	$3.2^{+1.5}_{-0.8}$	...	...	...	3.48 ± 0.14	14.7 ± 1.6	5.3 ± 0.4
2.95 ± 0.04	0.55 ± 0.05	2.7 ± 0.5	...	...	...	3.66 ± 0.11	15.9 ± 1.3	6.0 ± 0.4
3.10 ± 0.06	0.64 ± 0.03	2.6 ± 0.3	...	...	...	3.42 ± 0.06	14.1 ± 0.7	6.1 ± 0.2
3.29 ± 0.07	0.80 ± 0.03	2.12 ± 0.18	...	...	...	3.23 ± 0.09	16.3 ± 1.1	6.3 ± 0.4
3.50 ± 0.07	0.85 ± 0.03	2.14 ± 0.16	...	...	...	2.84 ± 0.08	17.4 ± 1.3	7.0 ± 0.5
3.70 ± 0.07	1.00 ± 0.03	1.83 ± 0.10	...	...	...	2.23 ± 0.09	15.7 ± 1.7	9.5 ± 0.5
3.89 ± 0.06	1.03 ± 0.03	1.90 ± 0.10	...	...	...	1.75 ± 0.09	12.6 ± 1.7	10.7 ± 0.7
4.12 ± 0.08	1.03 ± 0.03	1.90 ± 0.10	...	...	...	$1.49^{+0.24}_{-0.15}$	23^{+7}_{-5}	$7.0^{+2.0}_{-3.5}$
4.37 ± 0.08	1.22 ± 0.03	1.79 ± 0.08	...	...	...	$1.40^{+0.24}_{-0.16}$	23^{+10}_{-7}	9^{+2}_{-3}
4.71 ± 0.15	1.65 ± 0.03	1.81 ± 0.06	...	...	...	0.94 ± 0.12	11 ± 3	8 (fixed)
5.13 ± 0.10	1.61 ± 0.04	1.80 ± 0.08	...	...	...	<0.6	11 (fixed)	8 (fixed)

[a] Integrated between 0.1 and 1 Hz.
[b] Integrated between 1 and 100 Hz.

decreased from ~0.9% rms to ~0.4% rms. Above $S_z = 1.4$ its strength increased, to a peak value of ~1.3% rms at the NB/FB vertex. On the lower FB the strength decreased again, to a value of ~0.5% rms, and above $S_z = 3.0$ it increased to ~1.6% rms at the top of the FB. The index of the VLFN slowly increased from ~0.6 to ~1.0 between $S_z = 0.1$ and $S_z = 2.4$, with a small peak between $S_z = 1.6$ and $S_z = 1.9$, where the index had a value of ~1.5. Between $S_z = 2.4$ and $S_z = 3.2$, the VLFN was much steeper. The indexes were not well constrained and had values between 1.7 and 4.0. Above $S_z = 3.2$, where the error bars are much smaller, the index slowly decreased from 2.1 to 1.8.

Our fits did not require an additional component to fit possible HFN; no such component was found. Possible explanations for this are discussed in § 4.1.7.

3.3. *High-Frequency QPOs*

Both the lower and upper kHz QPOs were clearly detected; the lower kHz QPO between $S_z = 0.5$ and $S_z = 1.5$, the upper kHz QPO between $S_z = -0.3$ and $S_z = 1.7$. The results can be found in Table 8 and are shown in Figure 12. The QPO frequencies showed a clear increase with S_z, although both relations flattened at their low-fre-

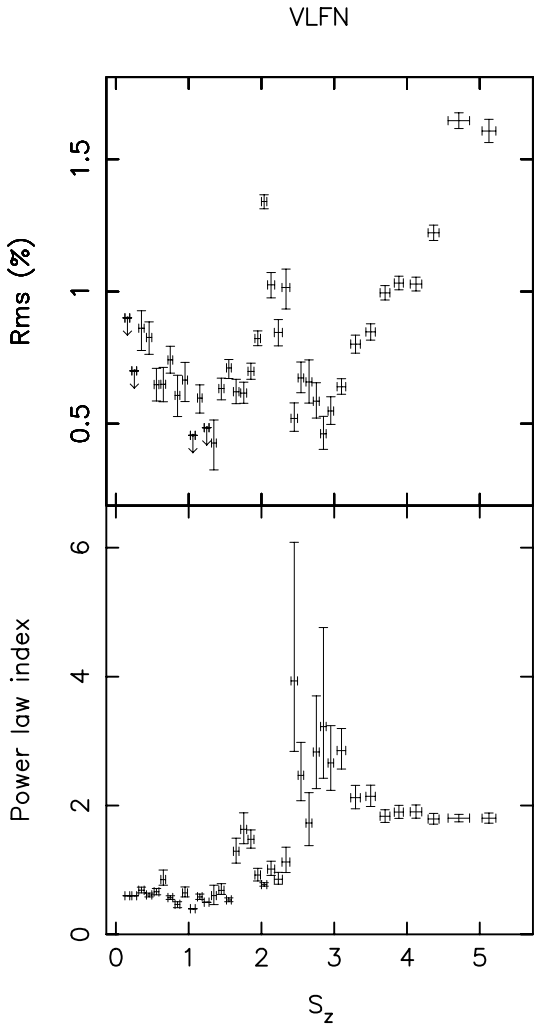

FIG. 11.—VLFN properties as function of S_z. The rms amplitude is the integrated power in the 0.1–1 Hz range. The arrows in the top panel represent upper limits.

quency ends. The FWHM of the lower kHz QPO was consistent with being constant at ~100 Hz, whereas the rms amplitude showed a peak near $S_z = 1.05$ with a value of 3.6 ± 0.3. The rms amplitude and FWHM of the upper kHz QPO both decreased with S_z.

Figure 13*a* shows the frequency difference of the two kHz QPOs as a function of the frequency of the upper kHz QPO. Some fits were made to the data; they are also shown in Figure 13*a*. The best fit to the frequency difference with a constant gave a value of 282 ± 4 Hz. The χ^2/degrees of freedom (dof) for this fit was 18.6/9, which means that at a 97% confidence level the frequency difference was not constant. This is the first time that this is observed for GX 17+2. Fits with first- and second-order polynomials (taking into account errors in both coordinates) resulted in, respectively, $\chi^2/\mathrm{dof} = 15.0/8$ and $\chi^2/\mathrm{dof} = 3.7/7$. Although the latter two fits show that with 99.76% confidence (3.2 σ) a decrease toward higher frequency is not monotonic, it is not clear either whether the decrease toward lower frequencies is significant or not. This would be the first time that such a decrease toward lower frequencies is observed in any kHz QPO source with a nonconstant frequency difference. To test this, two fits with a broken line (not shown) were performed, where in one case the slope of the low-frequency part was fixed to zero. They resulted in $\chi^2/\mathrm{dof} = 6.28/7$ (slope fixed) and $\chi^2/\mathrm{dof} = 2.52/6$ (slope free), which suggests that the frequency decrease toward lower frequency is significant at a 97.6% confidence level (2.4 σ).

In Figure 13*b* we show additional fits to the data with theoretical curves for the radial epicyclic frequency versus azimuthal frequency, which in the relativistic precession models are associated with the frequency difference and the upper kHz QPO frequency. The solid line is the best fit for circular orbits (Stella & Vietri 1998; Markovic & Lamb 2001), which yields a χ^2_{red} of 7.3 (dof = 9) for a mass of 2.07 $M_\odot$; the dashed line is the best fit for eccentric orbits (Markovic & Lamb 2001), yielding a χ^2_{red} of 1.14 (dof = 8) for a mass of 1.86 $M_\odot$. Both curves were calculated for nonrotating stars; rotation of the neutron star gives only insignificant improvements. For comparison we also plotted the data for Sco X-1 from van der Klis et al. (1997b). Clearly, both fits (especially the solid line) do not fit the decrease of the frequency difference toward lower frequencies, which occurs in a frequency range for the upper kHz QPO that was not observed in Sco X-1, very well.

The Q-values (frequency/FWHM) of the two kHz QPOs were consistent with each other and with that of the HBO and its harmonic (see Fig. 7); between $S_z = 1.0$ and $S_z = 1.5$, the Q-values of the HBO and kHz QPOs increased from ~5 to ~10. This unexpected finding may provide a key to understanding the formation mechanism of the three QPOs—this will be further discussed in § 4.1.5.

When comparing Figures 12 and 6, one can see that above $S_z = 1.5$, where the HBO frequency starts to decrease, the upper kHz QPO frequency still increases. In Figure 14 we plot the frequencies of both QPOs against each other. For values of the upper kHz frequency lower than 1030 Hz, the frequencies are well correlated, but above there is a clear anticorrelation. The solid line is the best power-law fit to the points below 1000 Hz. The power law index is 2.08 ± 0.07. This is the first time in any atoll or Z source showing kHz QPOs that an anticorrelation is observed between the frequencies of the low- and high-frequency QPOs (see § 4.1.2 for a discussion).

4. DISCUSSION

We performed a detailed study of the low- and high-frequency power spectral features of the neutron star low-mass X-ray binary and Z source GX 17+2. As was found in previous studies of GX 17+2 and other Z sources, the properties of most power spectral features correlated well with the position of the source along the Z track in the X-ray color-color diagram, suggesting that the spectral and variability changes are caused by one and the same parameter. Some new results were found, the most interesting being the fact that the frequency separation of the kHz QPOs was not constant and probably not monotonic (Fig. 13), that their Q-values were consistent with those of the HBO and its harmonic (Fig. 7), and that the frequency of the upper kHz QPO was anticorrelated with that of the HBO when the latter started to decline on the NB (Fig. 14). We also found a subharmonic of the HBO and showed that the absolute amplitude of the NBO/FBO is suppressed during type I X-ray bursts (Fig. 9). In the remainder of this section these and other results will be discussed in more detail. For a more detailed discussion, including a comparison of our results

TABLE 8
FIT RESULTS FOR THE HIGH-FREQUENCY QPOS

	Lower kHz QPO			Upper kHz QPO			
S_z	rms (%)	FWHM (Hz)	Frequency (Hz)	rms (%)	FWHM (Hz)	Frequency (Hz)	Difference (Hz)
-0.32 ± 0.04	...	...	...	<7	140^{+134}_{-68}	641^{+35}_{-20}	...
-0.23 ± 0.03	...	...	...	4.4 ± 0.6	100^{+46}_{-28}	637 ± 9	...
-0.15 ± 0.03	...	...	...	$5.4^{+1.0}_{-0.6}$	192^{+72}_{-45}	618 ± 12	...
-0.04 ± 0.03	...	...	...	5.7 ± 0.4	174 ± 25	650 ± 7	...
0.05 ± 0.03	...	...	...	5.5 ± 0.4	189 ± 29	663 ± 8	...
0.16 ± 0.03	...	...	...	5.4 ± 0.4	178 ± 26	678 ± 7	...
0.25 ± 0.03	...	...	...	5.8 ± 0.4	205 ± 24	689 ± 6	...
0.35 ± 0.04	...	...	...	4.8 ± 0.3	175 ± 21	722 ± 6	...
0.46 ± 0.04	<2.0	130 (fixed)	475 (fixed)	4.6 ± 0.2	164 ± 16	759 ± 5	...
0.56 ± 0.03	2.4 ± 0.4	145 ± 55	517 ± 18	4.4 ± 0.2	167 ± 18	780 ± 5	263 ± 18
0.65 ± 0.03	$2.7^{+0.4}_{-0.3}$	137^{+49}_{-30}	519^{+13}_{-9}	4.46 ± 0.20	160 ± 15	804 ± 4	284 ± 11
0.75 ± 0.03	1.6 ± 0.4	85 ± 59	530 ± 20	4.3 ± 0.2	181 ± 21	823 ± 7	293 ± 20
0.85 ± 0.03	2.4 ± 0.3	87 ± 25	555 ± 8	4.0 ± 0.3	154 ± 20	849 ± 6	294 ± 10
0.95 ± 0.03	3.1 ± 0.3	104 ± 25	607 ± 8	3.5 ± 0.4	156 ± 33	915 ± 11	308 ± 14
1.06 ± 0.03	3.6 ± 0.3	144 ± 24	655 ± 8	3.5 ± 0.3	149 ± 30	950 ± 8	294 ± 11
1.15 ± 0.03	2.9 ± 0.2	87 ± 15	682 ± 5	3.2 ± 0.4	200 ± 49	953 ± 14	271 ± 15
1.25 ± 0.03	$3.0^{+0.3}_{-0.2}$	112^{+27}_{-8}	714 ± 7	$2.4^{+0.4}_{-0.3}$	116^{+49}_{-33}	973 ± 11	258 ± 13
1.35 ± 0.03	2.0 ± 0.3	67 ± 24	752 ± 8	1.8 ± 0.4	115^{+106}_{-60}	1011 ± 24	259 ± 25
1.45 ± 0.04	2.0 ± 0.3	98 ± 41	794 ± 14	1.7 ± 0.3	61 ± 28	1033 ± 9	239 ± 17
1.55 ± 0.03	<2.3	80 ± 59	830 ± 19	1.8 ± 0.3	76 ± 32	1063 ± 13	...
1.65 ± 0.04	...	...	...	$1.8^{+0.5}_{-0.3}$	83^{+66}_{-37}	1087 ± 15	...
1.76 ± 0.04	...	...	...	<1.5	90 (fixed)	1085 (fixed)	...

with those obtained from other satellites (like *EXOSAT* and *Ginga*) and of other Z sources, we refer to Homan (2001).

4.1. *Timing Behavior*

4.1.1. *HBO and kHz QPO Models*

In our discussion of the HBO and kHz QPO results, we will consider only models that try to explain the behavior of both types of QPOs. Currently, these models are the relativistic precession model (RPM), the sonic point beat frequency model (SPBFM), and the two-oscillator model. In the latter model (see Osherovich & Titarchuk 1999), an angle between the magnetospheric equator and the disk plane is defined, which depends on the frequencies of the HBO and kHz QPOs and is supposed to be constant. However, Jonker et al. (2001) show, by using our GX 17+2 results and theirs of GX 5−1, that this is definitely not the case. For this reason, we will consider only the first two models. In the relativistic precession model (Stella & Vietri 1998, 1999; Morsink & Stella 1999; Stella, Vietri, & Morsink 1999), three frequencies are predicted; they correspond to the fundamental frequencies of motion of a test particle in the vicinity of a compact object and are identified with the HBO and the two kHz QPOs. The lowest predicted frequency, which should explain the HBO, is a factor of 2 lower than the low-frequency QPOs in the atoll sources and the subharmonic of the HBO in the Z sources. Hence, a way to produce second harmonics is required. Note that no actual mechanism is proposed for the production of QPOs themselves. However, in a recent model by Psaltis & Norman (2001) the accretion disk acts as low band-pass filter with resonances close to the three frequencies predicted in the RPM. It is unclear to what extent the details of the RPM (i.e., the turnover in the relation between HBO and upper kHz frequency) carry over to the Psaltis & Norman (2001) description. We also note that recent investigations of the RPM by Markovic & Lamb (2001) have cast some doubt on the frequencies predicted by the RPM and relations between them. In the sonic point beat frequency model (Miller, Lamb, & Psaltis 1998; Lamb & Miller 2001), the HBO is explained by the original beat frequency model of Alpar & Shaham (1985) and Lamb et al. (1985). The observed kHz frequencies are close to the orbital frequency at the sonic point of this disk and the beat of this frequency with neutron star spin frequency. The model requires the presence of a magnetosphere and a solid surface and can therefore not explain the low- and high-frequency QPOs in the black hole candidates.

4.1.2. *Horizontal Branch Oscillations*

The decrease of the HBO frequency on the NB in GX 17+2 was first observed in *RXTE* data that were not used in our analysis (Wijnands et al. 1996). There were interesting features in the HBO properties that were reproduced in that data and ours. In both cases the S_z dependence of the HBO frequency was not symmetric around its peak value; below, the frequency slowly flattened off to its maximum value, but above it showed a fast decrease by a few hertz that was followed by a more or less linear decrease with S_z. Also, simultaneously with the frequency drop, the FWHM increased by a factor of more than 2. Possible explanations for the HBO frequency decrease are discussed in § 4.1.4.

In all Z sources where a harmonic of the HBO has been observed, the frequency ratio of the harmonic and the fundamental is generally less than 2. This can be explained, at least in GX 17+2, by looking at the S_z dependence of the rms amplitudes of both components. In a certain S_z selection, both frequencies tend to be dominated by those with the higher rms amplitudes, and hence by lower S_z and lower

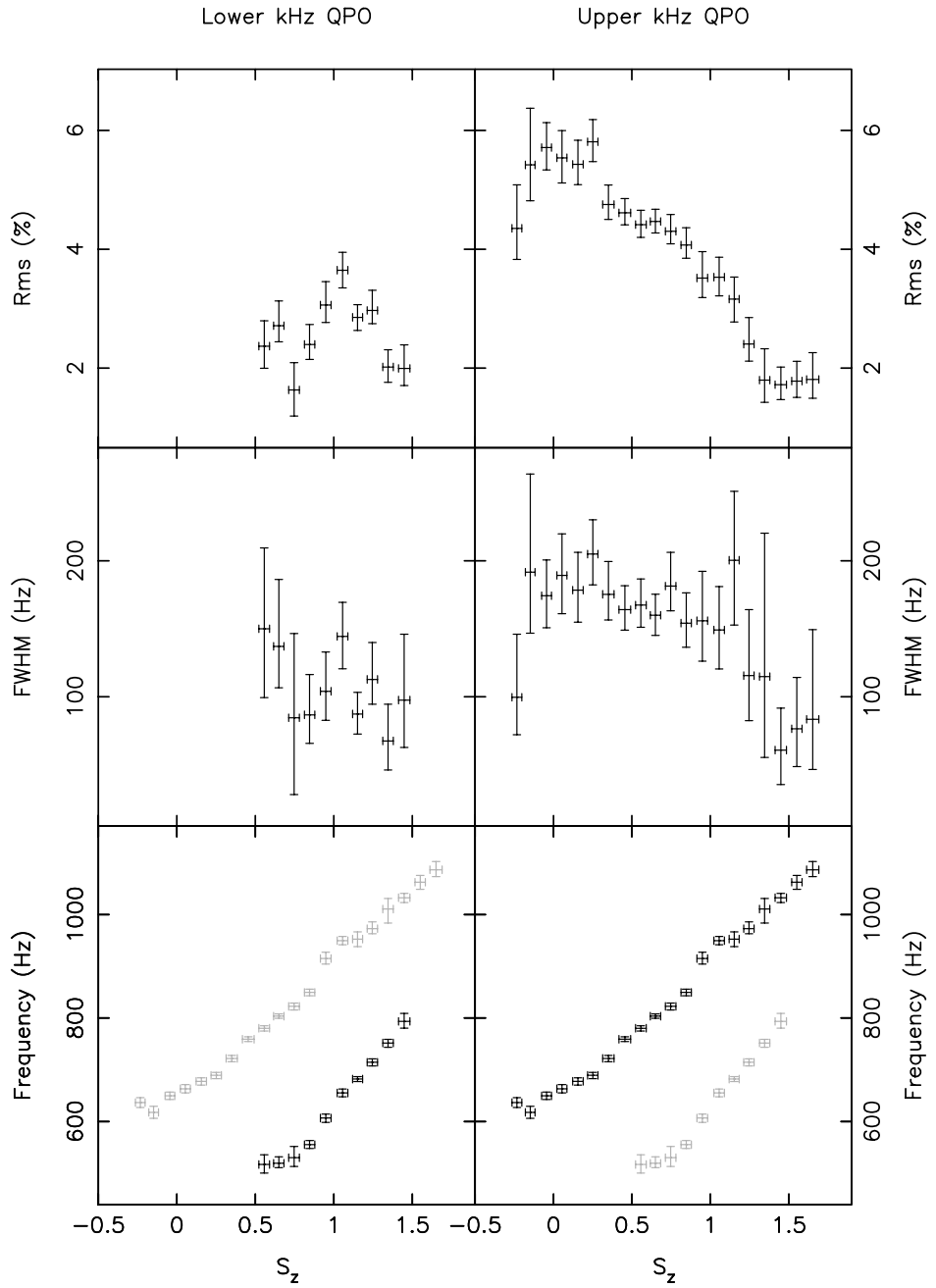

FIG. 12.—The kHz QPO properties as a function of S_z. For reasons of comparison, the frequency of the other QPO (*gray*) is also plotted in the frequency plot of each QPO.

frequencies; this effect will be stronger for the harmonic than for the fundamental, since the S_z dependence of its rms amplitude is steeper (see Fig. 6). As a result, the frequency ratio will end up to be less than 2. To test this hypothesis we calculated the weighted averages of two harmonically related linear functions, representing the HBO frequency–S_z relation between $S_z = 0.0$ and $S_z = 1.0$. As weight, we used linear functions that were fitted to the HBO rms–S_z relation between $S_z = 0.0$ and $S_z = 1.0$. The ratio of the weighted frequency averages was 1.93, which is very close to the observed value of 1.94.

Peaked features with frequencies intermediate to those of the LFN and the HBO have been reported for GX 340+0 (Jonker et al. 2000a), Sco X-1 (van der Klis et al. 1997b; Wijnands & van der Klis 1999a), GX 5−1 (Kuulkers et al. 1994; Jonker et al. 2001), and now also for GX 17+2. Based on the average frequency ratio of this sub-HBO component and the HBO in GX 17+2, 0.539 ± 0.015, we suggest that, similar to what was suggested for GX 340+0, it may be the subharmonic of the HBO. A comparative study by Wijnands & van der Klis (1999a) of low-frequency (HBO like) QPOs and band-limited noise components in the neutron star Z and atoll sources and black holes revealed strong correlations between the typical frequencies of those components. When plotting the frequency of the low-frequency QPO versus the break frequency of the band-limited noise, they found that the branch traced out by the Z sources, although lying parallel to that of the atoll source and black

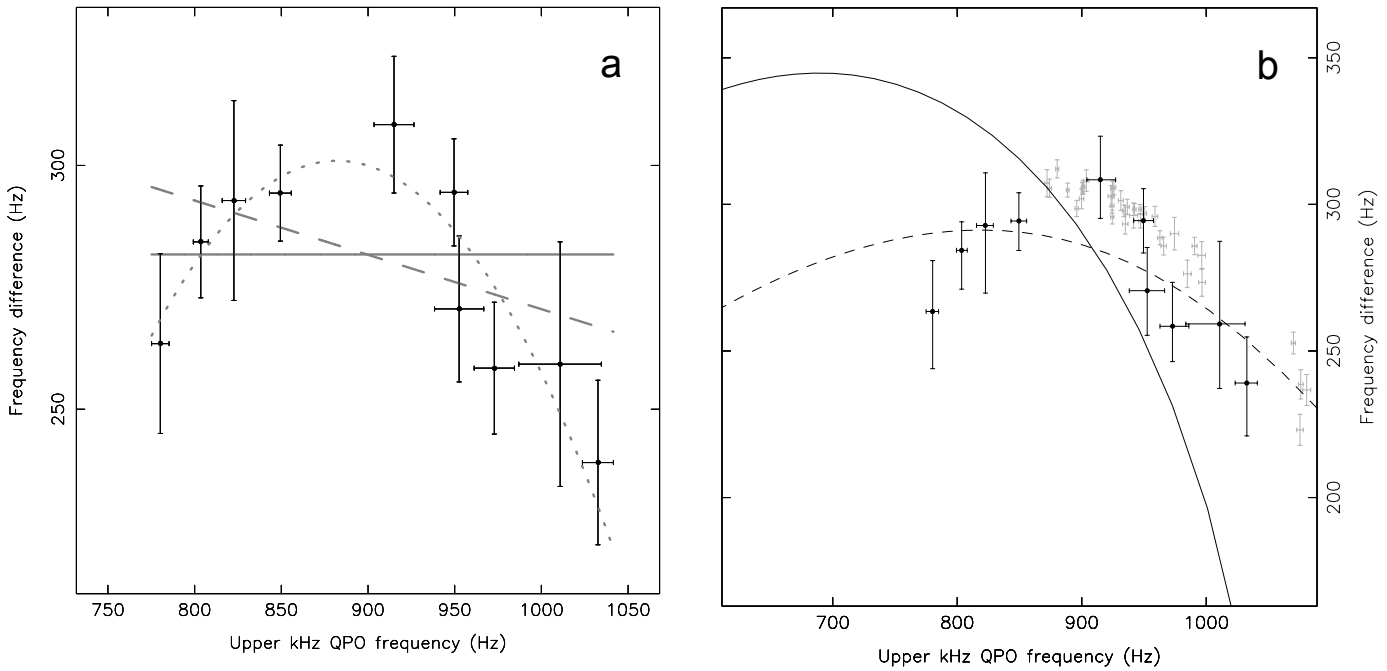

FIG. 13.—The kHz QPO frequency difference in GX 17+2 as function of the upper peak frequency. In (*a*) three fits to the data are shown (*gray*): a constant (*solid line*), a straight line (*dashed line*), and a parabola (*dotted line*). In (*b*) the two best fits to the data are shown for theoretical relations between the radial epicyclic frequency and azimuthal frequency: one for for circular orbits (*solid line*) and one for eccentric orbits (*dashed line*). The fits were kindly provided by D. Marković. Note that the dashed line requires highly eccentric orbits with apastron-to-periastron ratios of ~2–3. For comparison we also plotted the data for Sco X-1 (*gray*) from van der Klis et al. (1997b). For additional details see text.

holes, was slightly offset. It is interesting to see that this discrepancy between the Z sources on the one hand and the atoll sources and black holes on the other disappears (Jonker et al. 2000a), at least for GX 17+2, Sco X-1, and GX 340+0, when one uses the frequencies of the sub-HBO component, instead of the HBO frequency (see also Wijnands & van der Klis 1999a). If the low-frequency QPO in the atoll sources and the sub-HBO component of the three Z sources were indeed the same QPO, this would mean that the(se) Z sources do not anymore follow the relation between the low-frequency (HBO like) QPO and the lower kHz QPO as defined by atoll and black hole systems (Psaltis, Belloni, & van der Klis 1999). It is interesting to see that the three Z sources would then end up near or slightly above a second relation that is traced out by atoll sources like 4U 1728−34 and 4U 1608−52. At the moment, however, it seems that the relation found by Wijnands & van der Klis (1999a) and the main relation of Psaltis et al. (1999) are mutually exclusive for the two types of sources. Note that Wijnands & van der Klis (1999a) found that if in their plot for Sco X-1 the frequencies of the sub-HBO component and the HBO were used, instead of the LFN and HBO frequencies, the discrepancy between Sco X-1 and the non-Z sources also disappeared. This reinterpretation has the advantage of preserving the consistency with the Psaltis et al. (1999) relation as well.

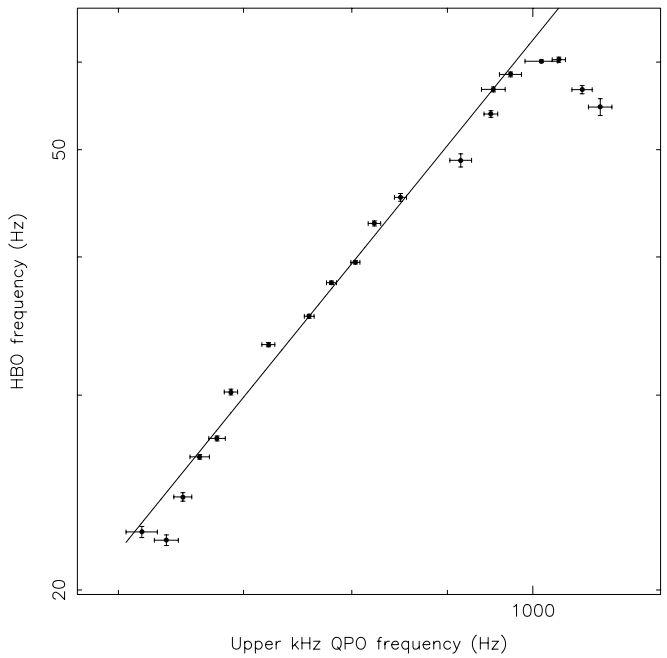

FIG. 14.—HBO frequency as a function of upper kHz QPO frequency. The solid line is the best power-law fit to the data below 1000 Hz for the upper kHz frequency. The power law index is 2.08 ± 0.07. A clear deviation from this relation can be seen for values above 1000 Hz.

The dominance of the even harmonics over the odd harmonics in the low-frequency (HBO like) QPOs, as suggested by the presence of a subharmonic of the HBO, not only is observed in the Z sources but also is a common feature in black hole candidates (BHCs) such as GS 1124−68 (Belloni et al. 1997) and XTE J1550−564 (Homan et al. 2001). It suggests that a twofold symmetry is present in the production mechanism of these low-frequency QPOs. For the SPBFM one could think of an asymmetry in the magnetic field, which results in different areas for the polar caps (see, e.g., Kuulkers et al. 1997). In the RPM a twofold symmetry is introduced by the two points at which the slightly inclined orbits of test particles cross the plane of the accretion disk.

4.1.3. *High-Frequency QPOs*

The kHz QPOs in GX 17+2 were discovered with *RXTE* (van der Klis et al. 1997a; Wijnands et al. 1997a). In our data the lower kHz QPO was found between 517 and 794 Hz ($S_z = 0.5$–1.5) and the upper kHz QPO between 618 and 1087 Hz ($S_z = -0.3$–1.7), similar to what was reported by Wijnands et al. (1997a). Our findings of the kHz QPOs in GX 17+2 are compatible with the general properties of kHz in other Z sources (van der Klis 2000).

An important new result is that the frequency difference is no longer consistent (at a 97% confidence level) with being constant (see Fig. 13). The frequency separation reached a maximum value of 308 Hz, when the upper peak frequency was about 915 Hz, and fell off in both directions to values of 263 and 239 Hz, when the frequencies of the upper peak were, respectively, 780 and 1033 Hz. Note that the decrease in both directions, when fitted with a parabola, resulted in significantly (3.1 σ) better fits than that with a constant. The decrease in the frequency separation at the low-frequency side of the upper kHz QPO, although itself only significant at a 2.3 σ level, has not been seen before in any kHz QPO source. In the other LMXBs that show a nonconstant frequency separation, Sco X-1 (van der Klis et al. 1997b), 4U 1608−52 (Méndez et al. 1998a, 1998b), 4U 1735−44 (Ford et al. 1998), and 4U 1728−34 (Méndez & van der Klis 1999), the frequency separation was not measured at upper peak frequencies as low as in GX 17+2. Although both the SPBFM and the RPM are capable of explaining the observed decrease in frequency difference toward higher upper peak frequencies, they have severe problems with a decrease toward lower frequencies. Such a decrease is not possible in the SPBFM, and, although it is in principle predicted by the RPM, that model yields reasonable fits to our data only when one allows for highly eccentric orbits (see Fig. 13*b*).

4.1.4. *HBO–kHz QPO Frequency Relation*

The principal aim of our observing campaign in 1999 was to check on the relation between HBO frequency (whose increase was known to turn into a decrease toward higher S_z) and upper kHz QPO frequency. Clearly, a decrease, or even flattening, of the upper kHz QPO frequency is not observed to accompany the decrease in HBO frequency (see Figs. 6, 12, and 14). In a pure RPM, this cannot be explained. However, if classical precession due to oblateness of the neutron star also plays a role, such an explanation is possible. For certain combinations of neutron star parameters, the prediction is that above a certain value of the upper kHz QPO frequency, the frequency of the HBO in fact starts to decrease (see Morsink & Stella 1999), because of the increasing importance of the classical precession. In GX 17+2 this turnover of the HBO frequency occurs at a value of ~1 kHz for the upper kHz QPO with a peak frequency of ~60 Hz for the HBO. Judging from Figure 2 in Morsink & Stella (1999), the relation between the HBO and upper kHz QPO frequencies in GX 17+2 would require a high neutron star spin frequency (~500–700 Hz), a neutron star mass of more than 2 $M_\odot$, and a hard equation of state (assuming the observed HBO frequency is 4 times the predicted frequency). In the RPM, well below the turnover, the HBO frequency is expected to scale quadratically with the upper kHz QPO frequency. The best power-law fit to the data below 1000 Hz yielded an index of 2.08 ± 0.07 (see Fig. 14), which is consistent with a quadratic relation.

In the SPBFM a turnover in the HBO–upper kHz QPO relation is not predicted, but since the two frequencies do not directly depend on each other, the model is flexible enough to account for it; if the turnover in HBO frequency could be explained by the two-flow model put forward by Wijnands et al. (1996), the steady increase of the upper kHz QPO frequency could in principle be explained by assuming that most of the radial flow falls back to the disk and rejoins the disk flow before the sonic point is reached, so that $\dot{M}$ at that location, and hence the upper kHz QPO frequency, keeps increasing. However, since the two radii at which the different QPOs are generated are very close, this seems a rather unlikely option.

4.1.5. *Q-Values of the HBO and kHz QPOs*

The Q-values of the kHz QPOs are remarkably similar to each other and to those of the HBO and its harmonic (see Fig. 7). They also show an almost simultaneous increase above $S_z = 1$, when the HBO harmonic is no longer detected. If the QPOs were artificially broadened by our selection method, averaging together peaks with different centroid frequencies, one would expect correlations of the FWHM (and Q-value) with the width of the S_z selection and with $d\nu/dS_z$. Such correlations, if present at all, are far too weak to explain the observed similarities.

The FWHM of a QPO can be caused by several mechanisms; intrinsic frequency variations, phase jumps, the simultaneous presence of several frequencies, and a finite lifetime of the signal will all cause a signal to appear as a broadened peak in a power spectrum. The data quality did not allow us to test the phase jump option. Lifetime broadening probably cannot explain our results. In the SPBFM there is no reason why the lifetimes of the low- and high-frequency oscillations, which are determined by different processes, would lead to similar Q-values. In the RPM, where all frequencies are generated by a single blob of matter, the lifetime for all variations should to first order be the same. However, in that case the Q-values of the kHz QPOs should be much higher (by a factor 10–20) than those of the HBO, since more kHz cycles fit in a blob's lifetime. Of course, it is possible that the lifetime of the oscillations is not determined by the lifetime of the blob but rather by a damping factor. Assuming that these factors are not the same for the different QPOs, the similarity of the Q-values could in principle be explained. However, there is no obvious reason why the (independent) damping factors would be fine-tuned in a such a way that they lead to similar Q-values.

Explaining the Q-values by broadening due to the presence of several frequencies does not work either. Below the turnover in the HBO–upper kHz QPO frequency relation, the frequency of the HBO scales quadratically with the frequency of the upper kHz QPO. A given range of upper kHz frequencies would therefore lead to a Q-value for the HBO that is half the Q-value for the upper kHz QPO. This is not consistent with what we find.

Frequency modulation could in principle explain the similar Q-values, but only if the modulation is caused by a different parameter than the one that determines the frequency changes along the Z track. Frequency modulation produces similar Q-values only if the QPO frequencies vary with the modulating parameter by the same factor, i.e., proportion-

ally to each other. The observed quadratic relation between the HBO frequency and that of the upper kHz QPO as well as the subsequent turnover shows that this is not the case for the parameter that causes the motion along the Z track. However, assuming that the modulating parameter is not responsible for motion along the Z (see § 4.2), we discuss the possibility of frequency modulation in a bit more detail. For broadening by frequency modulation to be observable in our power spectra, the timescale of these variations should be longer than that of the HBO. Additionally, the strength of those variations should anticorrelate with the Q-values of the QPO. Assuming that the parameter that causes the frequency modulations also causes some changes in the count rate, we could try to identify it in the power spectrum. The only reasonably strong components that we see in our power spectra and whose typical frequencies fulfill the above frequency requirement ($\nu < 10$ Hz) are the VLFN, the LFN, and the NBO/FBO. The VLFN might be associated with the motion along the Z (see § 4.1.7); disentangling that effect from a possible additional one on QPO frequencies is beyond the scope of this work. The strength of the LFN, which is of interest below $S_z = 1.5$, anticorrelates with the Q-values below $S_z = 1.5$. Above $S_z = 1.5$, the Q-values decrease again to a value between 2 and 5. In that case the broadening might be due to the appearance of the NBO/FBO and the increase in the LFN strength. It is interesting to note that in Sco X-1 it has already been found that the kHz QPO properties are clearly modulated by the NBO (Yu, van der Klis, & Jonker 2001).

4.1.6. *Normal and Flaring Branch Oscillations*

For the first time we were able to study the properties of the NBO/FBO during type I X-ray bursts. We found that the absolute rms amplitude significantly decreased when the radiation from the neutron star surface increased. This is clearly different from the behavior of the ~1 Hz QPOs in the dipping LMXBs 4U 1323−62 (Jonker, van der Klis, & Wijnands 1999), EXO 0748−676 (Homan et al. 1999), and 4U 1746−37 (Jonker et al. 2000b), whose absolute rms amplitudes increased during type I X-ray bursts. It is thought that these QPOs are not related to the NBO/FBO in the Z sources. The behavior of the NBO/FBO in GX 17+2 shows that NBO/FBO mechanism is very sensitive to the radiation field, thereby lending strong support for radiation feedback mechanisms (see below). In the framework of such mechanisms, it is easy to understand that the NBO/FBO disappears during bursts: the NBO/FBO is observed only in a narrow S_z range, suggesting that it requires a delicate balance of certain parameters, among which is the radiation field. The observations during the burst tails indicate that the NBO/FBO mechanism does not switch on instantly but rather becomes stronger in a more gradual way. Spectral fits during the bursts (Kuulkers et al. 2001) suggest that the spectral properties of the accretion flow itself are not affected much by the increase in radiation.

The frequency of the NBO/FBO changed from being more or less constant below $S_z = 2$ to being strongly correlated with S_z, above $S_z = 2$. In our data set we found the NBO between $S_z = 1.6$ and $S_z = 2.1$, although it may already have been present as a very broad feature as early as $S_z = 1.4$. Between $S_z = 2.0$ and $S_z = 2.1$, the NBO (6.86 Hz) was detected simultaneously with the FBO (13.9 Hz). Above $S_z = 2.1$ the FBO frequency increased, to ~23 Hz at $S_z = 2.65$. Note that the simultaneous presence of the NBO and FBO between $S_z = 2.0$ and $S_z = 2.1$ is likely an artifact of the S_z selection method. Inspection of dynamical power spectra showed that they were never present at the same time. It is interesting, though, that in that S_z selection their frequencies differed by a factor of 2, which is suggestive of mode switching of the NBO/FBO. However, there is evidence for QPOs with intermediate frequencies, which undermines that idea. The only way to see whether the frequencies really gradually transform into each other is to study the power spectral changes as a function of time. However, the quality of the GX 17+2 data is not sufficient to perform such a study.

The presence of the NBO/FBO in the Z sources has often been related to the fact that these sources accrete at near-Eddington mass accretion rates. It is thought that at these high mass accretion rates a significant fraction of the accretion flow is in the form of a thick and perhaps spherical flow. Also, the effects of radiation pressure are thought to play an important role in this regime. The model for the NBO by Fortner, Lamb, & Miller (1989) is based on a radiation feedback mechanism in a spherical accretion flow. Another model for the NBO was proposed by Alpar et al. (1992), in which the NBO frequency is basically that of sound waves in a thickened accretion disk. This model does not explain how the NBO changes into the FBO. A major problem for both models could be the recently discovered NBO/FBO-like QPOs in the two atoll sources 4U 1820−30 (Wijnands, van der Klis, & Rijkhorst 1999) and XTE J1806−246 (Wijnands & van der Klis 1999b). Certainly in the first source the luminosity is believed to be only ~20%–40 % of the Eddington luminosity, while near-Eddington luminosities are required in both models.

4.1.7. *Noise Components—LFN, VLFN*

The lack of HFN in our data, compared to, e.g., in the *EXOSAT* (Kuulkers et al. 1997) data, can be explained by instrumental effects and different approaches to fitting the data. A study of *EXOSAT* data of several sources by Berger & van der Klis (1994) showed that a component with an rms amplitude of ~3% is always present in the frequency range where the HFN was often found in the *EXOSAT* data. When HFN was found at lower frequencies, it was, based on strength and frequency, most likely the component that we identified as the subharmonic of the HBO.

Past measurements of the energy spectrum of the VLFN suggest that it is caused by motion of the source along the Z (van der Klis 1986, 1991; Lewin et al. 1992). The strength of the VLFN (Fig. 11) and the speed along the Z track ($\langle V_z \rangle$; see Fig. 3) should therefore have a similar dependence on S_z. Our results are inconclusive; although some correlations are observed (the increase above $S_z = 3$, and the steep increase around $S_z = 2$), there are also some differences. Most notable is the dip in the VLFN strength around $S_z = 3$, which is not observed as a decrease in $\langle V_z \rangle$. However, it is possible that because of the steepness of the VLFN around $S_z = 2.5$, most of its power was outside the range in which we determined the strength.

The LFN followed the behavior of the HBO, in both strength and frequency, until the latter disappeared ($S_z = 2.1$). Between $S_z = 2.1$ and $S_z = 2.8$, the behavior is rather complex and probably considerably influenced by the presence of the NBO/FBO. Above $S_z = 3.0$ the behavior

was rather clean, with a decrease in strength and an increase in frequency. It is not clear, however, whether the LFN on the FB is the same as that on the HB and NB. Unfortunately, no HBO was observed above $S_z = 2.1$ to compare its behavior with. Van der Klis et al. (1997b) suggested that in Sco X-1 the NBO/FBO emerged from the LFN. This seems not to be the case in GX 17+2, since the rms amplitude of the LFN already started to decrease well before the NBO appeared. Moreover, $\nu_{\max}$ shows a gradual increase between $S_z = -0.6$ and $S_z = 1.4$ to values well above the NBO frequency. A comparative study by Wijnands & van der Klis (1999a) strongly suggests that LFN has an origin similar to that of the band-limited noise component in atoll sources, BHCs, and the millisecond X-ray pulsar SAX 1808.4−3658. They suggest that this noise component is produced in the accretion disk and does not require the presence of a magnetosphere or solid surface.

4.2. *Broadband Spectral Behavior*

In our observations, GX 17+2 traced out the well-known Z-like tracks in the CD and HID. In addition to motion along this track, we observed secular motion of the Z track itself in the HID of epoch 3 (see Fig. 1), as was already reported by Wijnands et al. (1997a; see also Kuulkers et al. 1997, for a possible shift in the *EXOSAT* HID of GX 17+2). Below $S_z = 1$, the fluxes in the hard and soft energy bands behaved quite differently (Fig. 2); unlike the soft flux, the hard flux continued the trend that is observed above $S_z = 1$. Hence, the HB/NB vertex in the CD is entirely due to the turnover of the soft spectral flux. It is not clear what causes the soft spectral flux to decrease below $S_z = 1$. Although it is partly an instrumental effect—the peak of the soft component slowly shifts out of the PCA effective energy range as it becomes softer—most likely intrinsic source changes occur at $S_z = 1$. Most variability components increase in strength below $S_z = 1$, suggesting that they are related to the hard spectral component.

It is commonly believed that the motion of the source along and its position on the Z track are determined by the mass accretion rate ($\dot{M}$) through the inner accretion disk and onto the neutron star, increasing from the HB to the FB. Even though the count rates actually decrease on the NB and in some sources also on the FB (implying an anticorrelation between $\dot{M}$ and flux), there are several observational results that support this view: (1) The frequencies of the HBO and kHz QPOs, which in many models are directly related to $\dot{M}$, gradually increase from HB to NB (and in Sco X-1 even to the FB; see van der Klis et al. 1996). (2) The optical and UV flux increase from HB to FB (Hasinger et al. 1990; Vrtilek et al. 1990, 1991; van Paradijs et al. 1990; Hertz et al. 1992; Augusteijn et al. 1992); in X-ray binaries they are thought to be due to reprocessing of X-rays from the central source in the outer accretion disk. There are several reasons to believe that the optical and UV fluxes are betters tracers of the mass accretion rate than the X-ray flux (Hasinger et al. 1990). This would then solve the apparent anticorrelation between $\dot{M}$ and the (X-ray) flux (Hasinger et al. 1990). (3) Motion of a source is always along the Z track; jumps between branches are never observed, in accordance with the assumption that $\dot{M}$ varies continuously.

It has been found that secular motion of the Z tracks in the CDs of the Cyg-like sources does not affect the relation between the rapid variability properties and source position along the track (see, e.g., Kuulkers et al. 1994; Jonker et al. 2000a; however, see Wijnands & van der Klis 2001). In view of the $\dot{M}$-driven picture mentioned above, these changes cannot therefore be due to changes in $\dot{M}$ but should have a different origin. It has been suggested that the Cyg-like sources are viewed at a higher inclination than the Sco-like sources (Kuulkers et al. 1994). The differences in shapes of the Z tracks and some of the variability properties are also explained in this model (Kuulkers et al. 1994; Kuulkers & van der Klis 1995). Psaltis et al. (1995) suggest that the difference among the Z sources might be explained by a difference in the magnetic field strength, with the Sco-like sources having a lower magnetic field.

In the last few years, results have been obtained that may challenge the above described $\dot{M}$-driven picture. These results are mainly due to the arrival of *RXTE* and *BeppoSAX*, whose high-quality data revealed new phenomena and allowed for a better comparison between different classes of X-ray binaries. In the following we discuss how some of our results of GX 17+2 conflict with the $\dot{M}$-driven picture.

The frequency of the HBO in GX17+2 starts to decrease when the source is half-way through the NB. Although there are several explanations for this (see § 4.1.2), it means that the first assumption given above (i.e., QPO frequencies increase with $\dot{M}$) is not as solid as it seemed a few years ago.

The theory of type I X-ray bursts predicts that their properties change and correlate with $\dot{M}$ (Fujimoto, Hanawa, & Miyaji 1981; Fushiki & Lamb 1987). A study of the type I X-ray bursts in GX 17+2 by Kuulkers et al. (2001) showed that their properties did not correlate well with the position along the Z track at which they occurred and therefore not well with the inferred $\dot{M}$. Although other explanations are possible (see Kuulkers et al. 2001), this could mean that $\dot{M}$ does not determine the position of the source along the Z track. However, note that there does seem to be a correlation between burst occurrence and position along the Z track, which is usually explained by a changes in $\dot{M}$ onto the neutron star (along the Z track).

Recently, di Salvo et al. (2000) reported the discovery with *BeppoSAX* of a hard tail in the energy spectrum of GX 17+2. It increased in strength from the HB/NB vertex (where only upper limits on its strength could be determined) onto the HB. They also showed that the total 0.1–200 keV flux increased monotonically from the NB/FB vertex ($F_X = 1.52 \times 10^{-8}$ ergs s^{-1}) to the top of the HB ($F_X = 1.84 \times 10^{-8}$ ergs s^{-1}). This is different from the behavior of the 2.9–20.1 keV count rate (see Fig. 2*a*), which increased from NB/FB vertex to the HB/NB vertex but decreases afterward. As can be seen from Figure 2*b*, the behavior of the hard count rate confirms the findings of di Salvo et al. (2000). Also, there is no evidence for a change in its behavior near the HB/NB vertex. Unfortunately, no *BeppoSAX* data were taken on the FB to compare to our *RXTE* data. Hard power-law tails have also been found in the Z sources GX 5−1 (Asai et al. 1994), Cyg X-2 (Frontera et al. 1998; di Salvo et al. 2001a), Sco X-1 (Strickman & Barret 2000; D'Amico et al. 2001), and GX 349+2 (di Salvo et al. 2001b). Except for Sco X-1, where no clear correlation with spectral state was found (D'Amico et al. 2001), in all these sources the strength of the hard power-law tail seems to decrease in the same direction as was observed in GX 17+2, i.e., from HB to FB.

The behavior of the 0.1–200 keV flux on the NB and HB suggest that $\dot{M}$ actually increases in the opposite direction from what is commonly assumed. However, since the flux changes are rather moderate (~20%), other options are that $\dot{M}$ does not change at all along the Z track or at least that it shows no good correlation with the position along the Z. In that case, motion along the Z track (i.e., spectral change) is caused by another parameter, for example, the inner disk radius (van der Klis 2000). A similar possibility was suggested by Homan et al. (2001) to explain the observed behavior of the black hole transient XTE J1550−564. They found that spectral transitions occurred at different levels of the inferred $\dot{M}$. The spectral changes were ascribed to an unknown parameter, which they suggested to be the inner disk radius (based on variability), the size of the Comptonizing region (based on spectral hardness), and/or the accretion flow geometry (based on radio brightness). Note that options like the latter one may lead to changes in the $\dot{M}$ onto the neutron star, while the $\dot{M}$ through the inner disk remains constant; in that way the occurrence of type I X-ray bursts might become dependent on the position along the Z track. If the above also applies to the Z sources, the secular motion that is observed could perhaps be explained by changes in the $\dot{M}$. The apparent lack of a correlation between the type I burst properties and the position along the Z track could then also be explained, since $\dot{M}$ would determine the properties of the bursts but no longer the spectral properties.

It is interesting to see that GX 17+2 and the Z sources show in fact several similarities with XTE J1550−564 and other black hole sources. The first was already briefly mentioned above and concerns the independent behavior of the hard and soft flux on the HB. This independence of the hard and soft spectral components is commonly observed in BHCs (see Tanaka & Lewin 1995). Moreover, there are several properties that correlate well with the spectral hardness in BHCs and also with the spectral hardness in Z sources, which increases from the NB to the HB (for the moment we will exclude the FB from the comparison; it will be discussed later). These properties are the radio flux, the optical flux, and to a certain degree QPO frequencies. (1) The radio flux in BHCs is correlated with the spectral hardness (Fender et al. 1999; Fender 2001, and references therein). This is also true for GX 17+2, where the radio flux increases from the NB to the HB (Penninx et al. 1988). Sco X-1 (Hjellming et al. 1990a) and Cyg X-2 (Hjellming et al. 1990b) show similar behavior, whereas GX 5−1 only showed one radio flare on the NB (Tan et al. 1992). The behavior of the radio flux suggests that as the spectral hardness increases, part of the flow onto the neutron star evolves into an outflow. (2) Jain et al. (2001) found that in XTE J1550−564 the optical flux decreased during several small hard X-ray flares. Although the optical counterpart of GX 17+2 (Callanan, Filippenko, & Garcia 1999; Deutsch et al. 1999) has never been studied in much detail, this behavior is similar to the anticorrelation between the hard color and optical/UV flux on the NB and HB in the Z sources Cyg X-2 (Hasinger et al. 1990; Vrtilek et al. 1990; van Paradijs et al. 1990) and Sco X-1 (Vrtilek et al. 1991; Hertz et al. 1992; Augusteijn et al. 1992). (3) In XTE J1550−564, the frequencies of the low- and high-frequency QPOs anticorrelate with the hard flux (Sobczak et al. 2000; Homan et al. 2001). This is also found in GX 17+2 for the kHz QPOs and HBO (compare Fig. 2*b* with Figs. 6 and 12) and other Z sources. The only exception to this, together with the odd behavior of the hard tail in Sco X-1 (see above), is the correlation between the HBO frequency and spectral hardness that we observed on the lower NB. In that respect it is interesting to mention that Rutledge et al. (1999) report a switch from a correlation to an anticorrelation between the QPO frequency and spectral hardness in several BHCs, when the latter increases beyond a certain value. In addition to the QPO frequencies, the band-limited noise behaves similarly. It becomes stronger with spectral hardness, both in BHCs and Z sources (van der Klis 1995a).

It is tempting to compare the different black hole states (Tanaka & Lewin 1995; van der Klis 1995a) with those of the Z sources. Based on the above similarities, we suggest that the HB corresponds to the low state, the NB to the intermediate and/or very high state state, and the FB to the high state. However, there are still considerable differences: the low-state spectra are much harder than those of the HB, and the noise in the low state is much stronger. Moreover, flaring is not observed in the black hole high state. However, in both the high state and FB, the variability at high frequencies (>50 Hz) is extremely weak. It is not clear if and how the presence of a solid surface can account for these differences.

5. SUMMARY AND CONCLUSIONS

Our most important findings are the variable frequency difference of the kHz QPOs, the nonmonotonic relation between the HBO and the upper kHz QPO, the similar Q-values of the HBO, its second harmonic, and the kHz QPOs, and the suppression of the NBO amplitude during type I X-ray bursts.

In the following we summarize what the implications of each of our new findings are for some of the proposed models. The models that we considered for the HBO and kHz QPOs were the relativistic precession model (RPM), the "disk-filter" model, the sonic point beat frequency model (SPBFM), and the two-oscillator model. The latter model can be discarded on the basis of our results (see Jonker et al. 2001). For the disk-filter model, we assumed that it produces the same frequencies as the RPM, and it will therefore not be discussed separately.

1. HBO–kHz QPO frequencies: The RPM can explain a turnover of the HBO–kHz QPO frequency relation only when one assumes that the observed HBO is 4 times the predicted frequency and then only for rather extreme neutron star parameters: a high neutron star spin frequency (~500–700 Hz), a neutron star mass of more than 2 $M_{\odot}$, and a hard equation of state. The SPBFM needs some extension, for example, decoupling of part of the accretion flow from the disk flow outside the magnetosphere (to explain the HBO frequency decrease) and a subsequent recoupling of this flow with the disk flow before the sonic point radius is reached (to explain the increase in the kHz QPO frequencies). How this should exactly work is not clear.

2. Variable kHz QPO separation: Although not significant at a 3 σ level, the kHz QPO separation seems to decrease toward both low and high values for the upper kHz QPO frequency. The RPM basically predicts such behavior, but in its current form it is inconsistent with our results, as is apparent from Figure 13. The SPBFM cannot explain the possible decrease of the frequency separation on the low-frequency side.

3. Similar Q-values: In the SPBFM the low- and high-frequency QPOs are produced independently of each other, and there is no a priori reason why their Q-values should be similar. In the RPM, all the oscillations are produced by a single test particle. Lifetime broadening and the presence of multiple test particles both lead to different Q-values for the low- and high-frequency QPOs. Frequency modulation could work for both models, but only if the modulating parameter is not the same as the one that causes the motion along the Z track.

It is clear that both the RPM and SPBFM in their current forms cannot satisfactorily explain all the observed phenomena.

The observed behavior of the NBO during two type I X-ray bursts showed that this QPO is rather sensitive to the strength of the radiation field from the neutron star. This seems to confirm the basic idea behind the feedback mechanism model that was proposed by Fortner et al. (1989); i.e., it requires a delicate balance between the inward directed forces and the radiation field.

Finally, we compared the behavior of GX 17+2 (and the other Z sources) with that of (some) black hole LMXBs. Many similarities exist, particularly with regard to the relation between the hard spectral component on the one hand and variability properties (QPO frequency, broadband noise strength) and radio flux on the other. Based on recent findings in black hole LMXBs, we conclude that the mass accretion might not be the parameter that determines the position along the Z track after all.

This work was supported in part by the Netherlands Organization for Scientific Research (NWO) grant 614-51-002 and by NWO Spinoza grant 08-0 to E. P. J. van den Heuvel. R. W. was supported by NASA through the Chandra Postdoctoral Fellowship grant PF9-10010 awarded by the Chandra X-ray Center, which is operated by the Smithsonian Astrophysical Observatory for NASA under contract NAS8-39073. M. M. is a fellow of the Consejo Nacional de Investigaciones Científicas y Técnicas de la República Argentina. W. H. G. L. is grateful for support from NASA. The authors thank the referee for his/her thorough reading and useful remarks. Finally, we would like to thank Draza Marković for helpful comments and for providing theoretical fits to our data.

REFERENCES

Alpar, M. A., Hasinger, G., Shaham, J., & Yancopoulos, S. 1992, A&A, 257, 627
Alpar, M. A., & Shaham, J. 1985, Nature, 316, 239
Asai, K., Dotani, T., Mitsuda, K., Nagase, F., Kamado, Y., Kuulkers, E., & Breedon, L. M. 1994, PASJ, 46, 479
Augusteijn, T., et al. 1992, A&A, 265, 177
Belloni, T., van der Klis, M., Lewin, W. H. G., van Paradijs, J., Dotani, T., Mitsuda, K., & Miyamoto, S. 1997, A&A, 322, 857
Berger, M., & van der Klis, M. 1994, A&A, 292, 175
Bradt, H. V., Rothschild, R. E., & Swank, J. H. 1993, A&AS, 97, 355
Callanan, P. J., Filippenko, A. V., & Garcia, M. R. 1999, IAU Circ. 7219
D'Amico, F., Heindl, W. A., Rothschild, R. E., & Gruber, D. E. 2001, ApJ, 547, L147
Deutsch, E. W., Margon, B., Anderson, S. F., Wachter, S., & Goss, W. M. 1999, ApJ, 524, 406
di Salvo, T., et al. 2000, ApJ, 544, L119
———. 2001a, A&A, submitted
di Salvo, T., Robba, N. R., Iaria, R., Stella, L., Burderi, L., & Israel, G. L. 2001b, ApJ, 554, 49
Dieters, S. W., & van der Klis, M. 2000, MNRAS, 311, 201
Fender, R. 2001, Black Holes in Binaries and Galactic Nuclei, ed. R. Giacconi, L. Kaper, E. P. J. van den Heuvel, & P. A. Woudt (Berlin: Springer), 193
Fender, R., et al. 1999, ApJ, 519, L165
Ford, E. C., van der Klis, M., van Paradijs, J., Méndez, M., Wijnands, R., & Kaaret, P. 1998, ApJ, 508, L155
Fortner, B., Lamb, F. K., & Miller, G. S. 1989, Nature, 342, 775
Frontera, F., et al. 1998, in The Active X-Ray Sky: Results from BeppoSAX and RXTE (Amsterdam: Elsevier), 286
Fujimoto, M. Y., Hanawa, T., & Miyaji, S. 1981, ApJ, 247, 267
Fushiki, I., & Lamb, D. Q. 1987, ApJ, 323, L55
Hasinger, G., & van der Klis, M. 1989, A&A, 225, 79
Hasinger, G., van der Klis, M., Ebisawa, K., Dotani, T., & Mitsuda, K. 1990, A&A, 235, 131
Hertz, P., Vaughan, B., Wood, K. S., Norris, J. P., Mitsuda, K., Michelson, P. E., & Dotani, T. 1992, ApJ, 396, 201
Hjellming, R. M., et al. 1990a, ApJ, 365, 681
Hjellming, R. M., Han, X. H., Cordova, F. A., & Hasinger, G. 1990b, A&A, 235, 147
Homan, J. 2001, Ph.D. thesis, Univ. Amsterdam
Homan, J., Jonker, P. G., Wijnands, R., van der Klis, M., & van Paradijs, J. 1999, ApJ, 516, L91
Homan, J., Wijnands, R., van der Klis, M., Belloni, T., van Paradijs, J., Klein-Wolt, M., Fender, R., & Méndez, M. 2001, ApJS, 132, 377
Jahoda, K., et al. 1996, Proc. SPIE, 2808, 59
Jain, R. J., Bailyn, C. D., Orosz, J. A., McClintock, J. E., Sobczak, G. J., & Remillard, R. A. 2001, ApJ, 546, 1086
Jonker, P. G., et al. 2000a, ApJ, 537, 374
———. 2001, MNRAS, submitted
Jonker, P. G., van der Klis, M., Homan, J., Wijnands, R., van Paradijs, J., Méndez, M., Kuulkers, E., & Ford, E. C. 2000b, ApJ, 531, 453
Jonker, P. G., van der Klis, M., & Wijnands, R. 1999, ApJ, 511, L41
Jonker, P. G., Wijnands, R., van der Klis, M., Psaltis, D., Kuulkers, E., & Lamb, F. K. 1998, ApJ, 499, L191
Kuulkers, E., Homan, J., van der Klis, M., Lewin, W. H. G., & Méndez, M. 2001, A&A, submitted
Kuulkers, E., & van der Klis, M. 1995, A&A, 303, 801
———. 1996, A&A, 314, 567
Kuulkers, E., van der Klis, M., Oosterbroek, T., Asai, K., Dotani, T., van Paradijs, J., & Lewin, W. H. G. 1994, A&A, 289, 795
Kuulkers, E., van der Klis, M., Oosterbroek, T., van Paradijs, J., & Lewin, W. H. G. 1997, MNRAS, 287, 495
Kuulkers, E., van der Klis, M., & Vaughan, B. A. 1996, A&A, 311, 197
Lamb, F. K., & Miller, M. C. 2001, ApJ, 554, 1210
Lamb, F. K., Shibazaki, N., Alpar, M. A., & Shaham, J. 1985, Nature, 317, 681
Lewin, W. H. G., Lubin, L. M., Tan, J., van der Klis, M., van Paradijs, J., Penninx, W., Dotani, T., & Mitsuda, K. 1992, MNRAS, 256, 545
Markovic, D., & Lamb, F. K. 2001, MNRAS, submitted (astro-ph/0009169)
Méndez, M., et al. 1998a, ApJ, 494, L65
Méndez, M., & van der Klis, M. 1999, ApJ, 517, L51
Méndez, M., van der Klis, M., Wijnands, R., Ford, E. C., van Paradijs, J., & Vaughan, B. A. 1998b, ApJ, 505, L23
Miller, M. C., Lamb, F. K., & Psaltis, D. 1998, ApJ, 508, 791
Morsink, S. M., & Stella, L. 1999, ApJ, 513, 827
Osherovich, V., & Titarchuk, L. 1999, ApJ, 523, L73
Penninx, W., Lewin, W. H. G., Zijlstra, A. A., Mitsuda, K., & van Paradijs, J. 1988, Nature, 336, 146
Press, W. H., Teukolsky, S. A., Vetterling, W. T., & Flannery, B. P. 1992, Numerical Recipes in FORTRAN: The Art of Scientific Computing (2d ed.; Cambridge: Cambridge Univ. Press)
Priedhorsky, W., Hasinger, G., Lewin, W. H. G., Middleditch, J., Parmar, A., Stella, L., & White, N. 1986, ApJ, 306, L91
Psaltis, D., Belloni, T., & van der Klis, M. 1999, ApJ, 520, 262
Psaltis, D., et al. 1998, ApJ, 501, L95
Psaltis, D., Lamb, F. K., & Miller, G. S. 1995, ApJ, 454, L137
Psaltis, D., & Norman, C. 2001, ApJ, submitted
Rutledge, R. E., et al. 1999, ApJS, 124, 265
Sobczak, G. J., et al. 2000, ApJ, 531, 537
Stella, L., & Vietri, M. 1998, ApJ, 492, L59
———. 1999, Phys. Rev. Lett., 82, 17
Stella, L., Vietri, M., & Morsink, S. M. 1999, ApJ, 524, L63
Strickman, M., & Barret, D. 2000, in AIP Conf. Proc. 510, The Fifth Compton Symposium, ed. M. L. McConnell & J. M. Ryan (New York: AIP), 157
Tan, J., Lewin, W. H. G., Hjellming, R. M., Penninx, W., van Paradijs, J., van der Klis, M., & Mitsuda, K. 1992, ApJ, 385, 314
Tanaka, Y., & Lewin, W. H. G. 1995, in X-Ray Binaries, ed. W. H. G. Lewin, J. van Paradijs, & E. P. J. van den Heuvel (Cambridge Astrophys. Ser. 26; Cambridge: Cambridge Univ. Press), 126
van der Klis, M. 1986, in The Physics of Accretion onto Compact Objects, ed. K. O. Mason, M. G. Watson, & N. E. White (Lecture Notes in Physics 266; Berlin: Springer), 157

van der Klis, M. 1989, in Timing Neutron Stars, ed. H. Ögelman & E. P. J. van den Heuvel (NATO ASI Ser. C, 262; Dordrecht: Kluwer), 27
———. 1991, in Neutron Stars: Theory and Observation, ed. J. Ventura & D. Pines (NATO ASI Ser. C, 344; Dordrecht: Kluwer), 319
———. 1995a, in X-Ray Binaries, ed. W. H. G. Lewin, J. van Paradijs, & E. P. J. van den Heuvel (Cambridge Astrophys. Ser. 26; Cambridge: Cambridge Univ. Press), 252
———. 1995b, in The Lives of the Neutron Stars, ed. M. A. Alpar, U. Kiziloglu, & J. van Paradijs (NATO ASI Ser. C, 450; Dordrecht: Kluwer), 301
———. 2000, ARA&A, 38, 717
van der Klis, M., et al. 1997a, IAU Circ. 6565
van der Klis, M., Swank, J. H., Zhang, W., Jahoda, K., Morgan, E. H., Lewin, W. H. G., Vaughan, B., & van Paradijs, J. 1996, ApJ, 469, L1
van der Klis, M., Wijnands, R. A. D., Horne, K., & Chen, W. 1997b, ApJ, 481, L97
van Paradijs, J., et al. 1990, A&A, 235, 156
Vrtilek, S. D., Penninx, W., Raymond, J. C., Verbunt, F., Hertz, P., Wood, K., Lewin, W. H. G., & Mitsuda, K. 1991, ApJ, 376, 278
Vrtilek, S. D., Raymond, J. C., Garcia, M. R., Verbunt, F., Hasinger, G., & Kurster, M. 1990, A&A, 235, 162
Wijnands, R., et al. 1998a, ApJ, 493, L87
———. 1997a, ApJ, 490, L157
Wijnands, R., Méndez, M., van der Klis, M., Psaltis, D., Kuulkers, E., & Lamb, F. K. 1998b, ApJ, 504, L35
Wijnands, R., & van der Klis, M. 1999a, ApJ, 514, 939
———. 1999b, ApJ, 522, 965
———. 2001, MNRAS, 321, 537
Wijnands, R., van der Klis, M., Kuulkers, E., Asai, K., & Hasinger, G. 1997b, A&A, 323, 399
Wijnands, R., van der Klis, M., Psaltis, D., Lamb, F. K., Kuulkers, E., Dieters, S., van Paradijs, J., & Lewin, W. H. G. 1996, ApJ, 469, L5
Wijnands, R., van der Klis, M., & Rijkhorst, E. 1999, ApJ, 512, L39
Yu, W., van der Klis, M., & Jonker, P. G. 2001, ApJ, 559, L29
Zhang, W. 1995, XTE/PCA internal memo
Zhang, W., Jahoda, K., Swank, J. H., Morgan, E. H., & Giles, A. B. 1995, ApJ, 449, 930
Zhang, W., Strohmayer, T. E., & Swank, J. H. 1998, ApJ, 500, L167